

# A Review on Additive Manufacturing of Pure Copper

Qi Jiang<sup>1,2</sup>, Peilei Zhang<sup>1,2,3,\*</sup>, Zhishui Yu<sup>1,2,\*</sup>, Haichuan Shi<sup>1,2</sup>, Di Wu<sup>1,2</sup>, Hua Yan<sup>1,2</sup>, Xin Ye<sup>1,2</sup>, Qinghua Lu<sup>1,2</sup> and Yingtao Tian<sup>4</sup>

<sup>1</sup> School of Materials Engineering, Shanghai University of Engineering Science, Shanghai 201620, China; 13370297735@163.com (Q.J.); shc0010@126.com (H.S.); wudi612@126.com (D.W.); yanhua@foxmail.com (H.Y.); yexinsues@126.com (X.Y.); luqh@sues.edu.cn (Q.L.)

<sup>2</sup> Shanghai Collaborative Innovation Center of Laser of Manufacturing Technology, Shanghai 201620, China

<sup>3</sup> Fraunhofer Institute for Laser Technology ILT, 52074 Aachen, Germany

<sup>4</sup> Department of Engineering, Lancaster University, Bailrigg, Lancaster LA1 4YW, UK; y.tian12@lancaster.ac.uk

\* Correspondence: peilei@sues.edu.cn (P.Z.); yu\_zhishui@163.com (Z.Y.)

**Abstract:** With the development of the aerospace and automotive industries, high heat exchange efficiency is a challenge facing the development of various industries. Pure copper has excellent mechanical and physical properties, especially high thermal conductivity and electrical conductivity. These excellent properties make pure copper the material of choice for the manufacture of heat exchangers and other electrical components. However, the traditional processing method is difficult to achieve the production of pure copper complex parts, so the production of pure copper parts through additive manufacturing has become a problem that must be overcome in industrial development. In this article, we not only reviewed the current status of research on the structural design and preparation of complex pure copper parts by researchers using selective laser melting (SLM), selective electron beam melting (SEBM) and binder jetting (BJ) in recent years, but also reviewed the forming, physical properties and mechanical aspects of pure copper parts prepared by different additive manufacturing methods. Finally, the development trend of additive manufacturing of pure copper parts is also prospected.

**Keywords:** pure copper; additive manufacturing; selective laser melting; selective electron beam melting; binder jetting

## 1. Introduction

Copper and copper alloys are widely used in industry due to their excellent physical and chemical properties, such as thermal ( $400 \text{ W}/(\text{m}\cdot\text{K})$ ), electrical ( $58 \times 10^6 \text{ S}/\text{m}$ ) and corrosion resistance properties [1–4]. However, the physical properties of copper and copper alloys are seriously affected by impurity particles [5,6]. Pure copper material can avoid the influence of impure particles, thus providing more stable physical and chemical properties [7]. Due to its high thermal conductivity, electrical conductivity and machinability, pure copper is widely used in aerospace, automotive and electric fields [8]. In particular, pure copper is one of the main raw materials for heat exchangers and radiators, because of the high thermal conductivity [9–11]. In recent years, with the rapid development of the manufacturing industry and the electrical industry, the requirements for the geometrical complexity of the structure have gradually increased [12]. Traditional production methods are difficult to realize the processing of complex structures [13–15]. Recently, the technology of additive manufacturing (AM) can perfectly solve the problem that complex parts are difficult to produce [16–18].

During the last decades, AM technology developed rapidly. National Aeronautics and Space Administration (NASA) spent a lot of time researching additive manufacturing techniques [16]. The AM technology is expected to become the dominant processing method, in combination with computer aided design (CAD) [19,20]. AM is a technique in which materials are stacked layer by layer to form a part [21,22]. In recent years, with the development of AM technology, many processing methods have been proposed, such as extrusion, melting, light curing and spraying, etc. [23]. In general, the heat sources used in additive manufacturing are laser beam and electron beam [24–26]. Two powder bed fusion (PBF) techniques are the main stream of AM [27], selective laser melting (SLM) and selective electron beam melting (SEBM), respectively [28]. In addition, there are many other additive manufacturing methods, such as binder jetting (BJ) [29], laser metal deposition (LMD) [30] and ultrasonic additive manufacturing (UAM) [31]. Recently, additive manufacturing technology has been widely used in steel, copper, titanium and other metal materials processing and manufacturing [10,32].

---

Lehnert et al. [33] studied the microstructure and mechanical properties of high-alloy quenching and partitioning TRIP steel, which was processed by EBM. RANEY®-type copper catalyst for methanol synthesis was manufactured by laser metal deposition (LMD). This is the work of Heßelmann et al. [34]. The microstructure and properties of Ti-6Al-4V fabricated by low-power pulsed laser directed energy deposition had been researched by Tan et al. [35]. Sridharan et al. [36] studied the forming mechanism of UAM additive manufacturing technology. They analyzed the microstructure of the Al-Ti joint produced by UAM additive manufacturing technology and observed the texture evolution. They concluded that the joint forming mechanism of UAM additive manufacturing is the formation of severe shear deformation at the interface.

Pure copper has excellent physical and chemical properties, so researchers spend a lot of energy on additive manufacturing of this material [37]. At present, a variety of additive methods have been selected by the researchers for pure copper additive manufacturing to study the microstructure and properties. Walkera et al. [24] used SLS to produce copper parts and analyzed their microstructure and mechanical properties by comparing the analysis data with that of other additive manufacturing parts, the parts produced by SLS after a homogenization treatment. The mechanical property of the samples showed that the strength and ductility were close to those of the sample produced using other techniques. Zhong et al. [30] produced the additive parts of pure copper by LMD. After analysis and verification, the Cu<sub>2</sub>O precipitation phase was found in the parts, which were manufactured in an environment of unprotected gas. Due to the presence of the nano-sized Cu<sub>2</sub>O precipitation phase, the microhardness of the sample was obviously improved. Raab et al. [38] produce pure copper parts via SEBM. By testing the thermal and electrical conductivity, the impure particles are found to have a bad effect on the physical and chemical properties. No matter what kind of additive manufacturing method is used to produce the parts, the main purpose is to ensure the physical and chemical properties of the parts are in good shape. In order to further improve the performance of the parts, various post-processing methods were tested, such as abrasive polishing and hot isostatic pressing (HIP) [19,25]. In the process of additive manufacturing, the tested also found many factors affecting the performance of pure copper parts, but few reviews have summarized them. Therefore, this paper will use PBF additive manufacturing techniques to introduce the performance of its production components.

The aim of this paper is to review the status of pure copper additive manufacturing and performance evaluation of the additive parts. This article reviews the structural design and forming control of pure copper parts manufactured by additive manufacturing with SLM, SEBM and BJ technologies. The mechanical properties and physical properties of the formed parts are evaluated. In addition, the factors affecting the performance differences are discussed. The prospects and challenges of additive manufacturing pure copper parts are also proposed. The study of additive manufacturing pure copper via SLM, SEBM and BJ was shown in Table 1.

**Table 1.** Study on additive manufacturing of pure copper SLM, SEBM and BJ.

Method	Power (W)	Scanning Speed (mm/s)	Layer Thickness ( $\mu\text{m}$ )	Hatch ( $\mu\text{m}$ )	Energy ( $\text{J}/\text{mm}^3$ )	Density (%)	Electric Conductivity (%IACS)	Thermal Conductivity ( $\text{W}/(\text{m}\cdot\text{K})$ )	Tensile Strength (MPa)	Micro Hardness (HV)	Grains Size ( $\mu\text{m}$ )	Year/Ref.
SLM	300	400	30	50	500	84	-	-	-	-	-	2019 [39]
	800	400	30	90	741	98	$88 \pm 2$	$336 \pm 7$	-	-	-	
	800	400	30	70	952.38	98	$86 \pm 3$	$329 \pm 11$	-	-	-	
	600	200	30	90	111.1	98	$83 \pm 3$	$317 \pm 12$	-	-	-	
	800	300	50	25	2133.3	95.7	-	-	-	-	-	
	800	300	50	40	1333.3	95.9	-	-	-	-	-	
	800	300	50	50	1066.67	95.5	-	-	-	-	-	
	800	300	50	75	711.1	96.4	-	-	-	-	-	
	800	300	50	100	533.3	96.6	-	-	-	-	-	
	800	300	50	120	444.4	96	-	-	-	-	-	
	195	400	30	80	203	$83.01 \pm 0.13$	-	-	-	-	15–75	2017 [5]
	190	400	20	60	395	82	-	-	-	61.48	-	2019 [40]
	500	400	30	90	462.96	98.8	89	-	270	93	-	2020 [7]
	200	400	30	80	208.3	$99.1 \pm 0.5\%$	-	-	$248 \pm 8.5$	$84 \pm 4.2$	-	2020 [41]
	200	100	50	120	333.3	88.1	-	-	149	-	-	2016 [10]
	200	300	45	50	296.3	85.8	50.3	-	-	-	5–50	2019 [27]
	800	300	50	100	533.3	96.6	-	-	-	-	-	2020 [37]
	125	2000	30	20	104.2	64.1	-	-	-	-	-	-
	100	600	30	20	277.78	69.3	-	-	-	-	-	-
	75	300	30	20	416.67	69.5	-	-	-	-	-	-
150	900	30	20	277.78	71	-	-	-	-	-	-	
75	900	30	20	138.89	63	-	-	-	-	-	-	
725	400	30	120	503.47	98	39	-	$125 \pm 11$	-	-	-	
650	1000	30	120	180.5	94.7	-	-	-	-	-	-	
600	1500	50			97	-	-	-	-	-	-	
200		35	10		91.2	-	-	-	-	-	-	
800	600	50	100	266.67	96.74	-	-	-	-	-	-	
275	250	50	100	220	99.5	94	403.55	-	-	-	-	
450	500	50	100	180	99.5	-	-	$177 \pm 3.3$	-	-	-	
600	1000	50	100	120	99.5	-	408.27	-	56.6 $\pm$ 2.53	-	-	
850	1500	50	100	113	-	100	411.89	-	55.5 $\pm$ 1.64	-	-	
1100	2000	50	100	110	99.5	100	385.64	-	57.8 $\pm$ 1.55	-	-	
-	3000	50	100	80	99.831	96.24	400.1	-	-	-	-	

	450	500		100		99.5	-	-	231.6 ± 5.4	-	-	2020 [28]
	-	3000	50	100	0.275	99.5	-	-	-	-	10-50	2015 [47]
	-	80	-	-	-	-	-	--	-	88	60	2011 [48]
	-	-	-	-	-	99.32	97	390	76	-	-	2014 [49]
	-	-	-	-	-	77.7	51.72	245.7 ± 4.7	82.0 ± 5.3	-	-	
	-	-	-	-	-	82.4	63.79	256.5 ± 4.4	129.3 ± 0.9	-	24.1	
	-	-	-	-	-	83.6	65.52	262.3 ± 8.2	115.8 ± 9.2	-	22.3	
	-	-	-	-	-	85.8	63.79	266.3 ± 18.5	135.3 ± 13.7	-	34	2019 [50]
	-	-	-	-	-	90.5	81.03	293.5 ± 5.5	144.9	-	13.4	
	-	-	-	-	-	97.3	89.65	327.9 ± 7.1	176.4 ± 6.5	-	25.8	
BJ	-	-	-	-	-	75.22	-	247.26	7.67	-	-	
	-	-	-	-	-	84.44	-	291.28	35.04	-	-	
	-	-	-	-	-	94.6	-	310.78	56.53	-	-	
	-	-	-	-	-	93.92	-	297.14	41.71	-	-	2020 [51]
	-	-	-	-	-	82.64	-	271.12	30.77	-	-	
	-	-	-	-	-	87.7	-	278.1	24.29	-	-	
	-	-	-	-	-	92.61	-	294.51	45.85	-	-	

## 2. Pure Copper Additive Manufacture Methods

PBF technology is a common technique in 3D printing, which can be divided into two types according to different heat sources [52–54]. Additive manufacturing technologies with laser as heat source include SLS, SLM, etc., and with electron beam as heat source include SEBM, EBDM, etc. [55,56]. SLM and SEBM account for 82% of the total PBF. The ASTM/ISO 52900 standard had defined the PBF technology [57]. This standard specifies that the thickness of the powder layer is between 20 and 100  $\mu\text{m}$ , which is cut into layer by layer in a CAD model and then printed into a 3D part under the action of heat source [58–60]. In this section, the research status of two most representative PBF technologies (SLM and SEBM) is introduced in detail. At the same time, we will also introduce a technology similar to PBF, namely BJ technology. The basic principle of this technology is similar to that of PBF technology. The biggest difference is the way to obtain finished parts. This technology will be described in detail later.

### 2.1. Selective Laser Melting

SLM technology is a kind of PBF additive manufacturing technology, which takes laser as the heat source [62–64]. In the SLM process, the additive results are affected by parameters, such as laser power, defocusing amount (spot size), scanning trajectory, scanning speed, layer spacing, etc. [65–67]. A schematic diagram of SLM technology is shown in Figure 1. After focusing the laser light on the XY scanning mirror through the lenses, the position of the laser light is adjusted by the deflection of the XY scanning mirror. The parts are sliced by CAD model and printed layer by layer. After each layer is finished, the powder layer is relaid by leveling roller [17,68]. SLM technology has many advantages, such as fast processing speed, high process flexibility and high material utilization rate, which make SLM technology widely used [14,69]. Therefore, pure copper parts produced by SLM technology are used in various fields. Wang et al. [70] used SLM technology to produce pure copper hydrophobic layer on steel surface. In this study, due to the high flexibility of SLM technology, coatings with a contact angle as high as  $160^\circ$  and sliding angle as low as  $3.9^\circ$  were successfully produced.

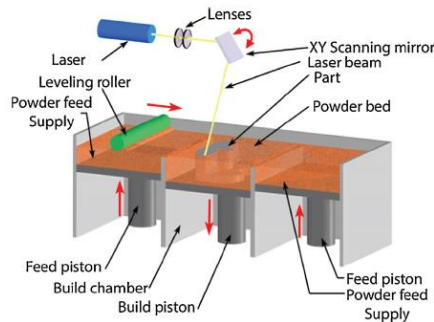


**Figure 1.** Schematics of additive manufacturing (AM) by selective laser melting (SLM) [61].

Pure copper has the advantage of excellent physical properties, but also has the extremely high reflectivity on laser in molten state and liquid state [28,38]. Commercially available SLM devices use lasers with wavelengths in the range of 1000–1100 nm. Within this range, however, pure copper reflects as much as 98% of the laser [26,28]. Many scholars have pointed out the harm of laser reflection. In the study of Jadhav et al. [39], they subjected the optical coating to unprotected exposure for 12 h while a laser with a wavelength of 1080 nm was repeatedly scanned over a 90% reflectivity copper substrate. The damage of optical coating after 12 h reflection is shown in Figure 2. The image shows the apparent peeling of the coating, which demonstrates the damage done to the optical elements by the reflected laser. In addition, high reflectivity also leads to energy loss, resulting in insufficient heat input. In order to solve the problem of insufficient heat input caused by laser reflection, the researchers have taken different approaches, such as using high-power single-mode fiber laser [8,43], use other wavelength or frequency laser to increase the absorption rate [71] or other elements added in the powder to increase the absorption rate of laser [1].

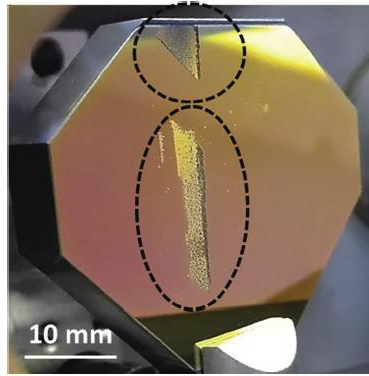


**Figure 2.** The damage to the optical mirror [39].

Copper can absorb laser wavelengths of 515 nm more easily than 1000 nm. The absorption rate of metal to the laser is up to 25–40% [1,5,28]. Therefore, adopting green laser as copper SLM 3D printing energy can reduce the need for laser energy and provide focusing accuracy. In the research of Prasad et al. [71], in order to maintain the necessary heat input, compared with additively manufactured aluminum, steel and titanium, they use the largest power (1 kw) and the smallest speed (0.1 m/min). Other researchers are developing SLM technologies for blue and red lasers, but not much research has been done on pure copper [72,73].

## 2.2. Selective Electron Beam Melting

SEBM technology as another PBF technology, its principle is basically the same as SLM technology [4,25,74]. As shown in Figure 3, SEBM technology also builds part models by means of 3D modeling, and then produces them layer by layer through selective melting of electron beams [75–77]. Different from SLM technology, the heat source used by SEBM is electron beam, and the influence of electron beam through electromagnetic coils makes the electron beam select the change of melting region [78–80]. In addition, SEBM technology has many advantages, such as: High vacuum, which avoids oxidation of parts during manufacturing; Low reflectivity, which makes it suitable for processing high reflectivity materials; In most cases, there is no heat treatment because the SEBM additive requires preheating of the substrate; Higher power can be used to ensure higher processing rates [81,82].

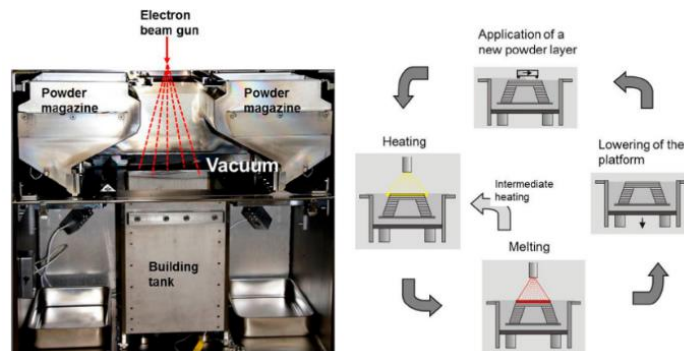


**Figure 3.** The SEBM process. Left: Process chamber. Right: 4-step process for building one layer [25].

At present, SEBM technology is applied in various fields, such as artificial skeletons, aerospace and so on [78,80]. The SEBM technology will be very suitable for the processing of high reflectivity materials due to the different ways in which materials reflect electrons and photons [83]. Therefore, SEBM technology can solve the problem of high reflectivity of copper in molten state. It has attracted the attention of many researchers. Moreover, in the case of pure metal additive manufacturing, it is sensitive to the influence of pollutants, especially the influence of oxygen on the performance of parts [84–86]. The technology of SEBM can avoid the influence of oxygen in the environment because it is carried out in a vacuum condition [87]. However, the oxidation of pure copper powder is inevitable during transportation and storage. Guschlbauer et al. [28] have done research on this. They produced parts by using powders with different oxygen content and studied the effect of oxygen

content on the performance of parts. Finally, it was proved that excessive oxide content will cause cracks and other defects, which will seriously affect the performance of the parts.

### 2.3. Binder Jetting

BJ technology, a type of additive manufacturing technology, originated in the 1990s from the Massachusetts Institute of Technology [88–90]. BJ additive manufacturing technology is based on PBF technology, but there are some differences in equipment [91]. Figure 4 shows the schematic diagram of BJ technology. We can see that the printing system is made up by a printhead, a powder spreader, a heating lamp, and a print feed bed [88]. The printing process is the main difference between BJ technology and other additive manufacturing technologies [92]. When the powder is laid on the printing bed, unlike PBF technology, the print head will not emit a high-energy beam according to the planned path to melt the powder, but spray the binder. Then the heating lamp will move to the position where the binder was sprayed for heating and curing [92,93]. When the bonded parts were depowdered, the parts were placed in a high temperature furnace for sintering and pyrolyze the binder [94].

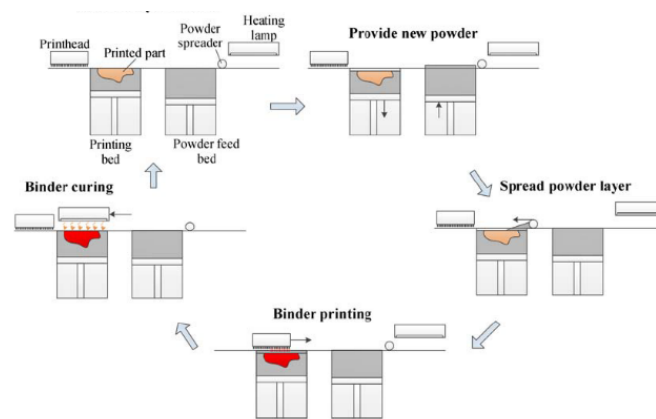


**Figure 4.** The schematics of BJ-AM process steps [88].

With the development in recent years, BJ technology has been widely used in various materials, such as metals and ceramics [95]. In the current research, additive manufacturing of metals attracts more attention. The BJ technology has been applied to copper, iron, aluminum and other pure metals and alloys [90,92]. Wheat et al. [89] have studied the effect of titanium alloy powders with different particle sizes on the density change of parts produced by BJ additive technology. It is found that the density of the parts with finer particle powder changes greatly after sintering, which also means that a large anisotropy will be produced. In the research of Gonzalez et al. [91], the characteristics of ceramic parts made by BJ additive technology are discussed. Finally, parts with a relative density of up to 96% are obtained, which creates opportunities for BJ technology to be applied in medical fields. BJ additive technology develops rapidly due to its special advantages [50]. Compared with common PBF technology, it has the following advantages: 1. There is no size limit for production parts; 2. No supporting structure is required; 3. Wide range of applicable materials, no need to pay attention to physical properties such as melting point reflectivity of materials, and can be mixed with different materials; 4. Low price of equipment, no need to close the cavity; 5. Low powder requirements [19,95]. The special processing technology of BJ additive technology is suitable for the processing of high reflectivity materials and provides a new option for the processing of pure copper additives [50,95]. As early as 2015, Bai et al. [96] explored the feasibility of producing pure copper components with BJ additive technology. The article talks about the changes in density, shrinkage and tensile strength of parts produced by different powders. Finally, the complex structural parts as shown in Figure 5 were obtained by adjusting the process parameters. The maximum density of parts manufactured by BJ additive technology is 85.5%. The density of parts produced by BJ additive manufacturing technology is too low, so the tensile strength of parts is lower than that of pure copper parts produced by traditional processing methods. The density ratio is low due to the addition of a large amount of binder during the production of parts via BJ additive manufacturing technology. During the sintering process, a large number of holes are left after the binder is heated and decomposed, thereby reducing the density of the part [97]. At the same time, the existence of pores reduces the performance of the part.



Figure 5. Complex-shaped copper made via binder jetting [19].

### 3. Performance of Pure Copper 3D Printed Parts

#### 3.1. Structure Design

The rapid development of AM technology provides a new method for manufacturing complex structural parts, and it has attracted extensive attention of researchers due to its advantages of high material utilization rate and high degree of freedom [98–100]. After more than 20 years of development, AM technology can produce complete parts without special tooling and expensive traditional processes, and has penetrated into various industries, such as construction, medicine, automobiles, aerospace, etc. [11]. The principle of AM layered manufacturing can simply create complex channels inside a part, increasing the surface area of the part. Pure copper has good thermophysical properties, so it is very attractive for heat exchanger applications [43,101].

The excellent thermophysical properties of pure copper combined with the ability of AM technology to manufacture complex parts have attracted more attention from researchers [11,102]. Tang et al. [64] used SLS additive technology to produce complex pure copper parts with a density of 76% and a surface roughness of 16–21  $\mu\text{m}$ , which could not meet the standard of use. The SLS additive technology is only the sintering of powder rather than the complete melting of powder, so it is unavoidable that the density does not reach the required value. The researchers therefore focused on the SLM additive technique by completely melting the powder. In the research of Gradla et al. [16], it was mentioned that NASA used GRcop-alloy to manufacture channel-cooled combustion chambers and passed the test, the part reached the standard that can be used. Compared with pure copper, copper alloy has better processability but worse performance, so the research on additive manufacturing a complex structure of pure copper is more attractive. In the study of Constantina et al. [13], complex pure copper components were fabricated by SLM technique. The heat sink produced by the authors is shown in Figure 6, in which Figure 6a is the commercial heat sink for comparison with other heat sinks manufactured by SLM. After comparative testing, it is found that the heat dissipation effect of the same form of heat sink is similar to the commercial, and the heat dissipation effect of the helix and bent tubes heat sink is better. It is worth mentioning that the bent tubes heat sink has a pore diameter of only 1 mm and a wall thickness of only 300  $\mu\text{m}$ . This result also provides a new idea for micro additive manufacturing. For example, Wang et al. [70] used SLM additive technology to produce nanoscale surface coatings, which provided a new method for the production of surface hydrophobic layers. Although the technology of pure copper additive using laser as a heat source is developing continuously, there are still some problems. For example, in the research of Gu et al. [103] and Zhu et al. [104], the influence of powder spheroidization during laser processing is mentioned, and the spheroidization of powder will affect the surface forming condition of parts. In the study of Sinico et al. [73], the influence of powder particle size distribution on forming parts was mentioned. In this paper, the parts with forming density of 98.1% were obtained by using powder with particle size range of 10–35  $\mu\text{m}$ , and by comparing with powder with particle size range of 15–45  $\mu\text{m}$ , it was found that the forming density of fine powder was higher. Although there have been many studies on the production of pure copper parts through SLM additive manufacturing technology in recent years, it is still a challenge to produce crack-free and dense parts [10,39].

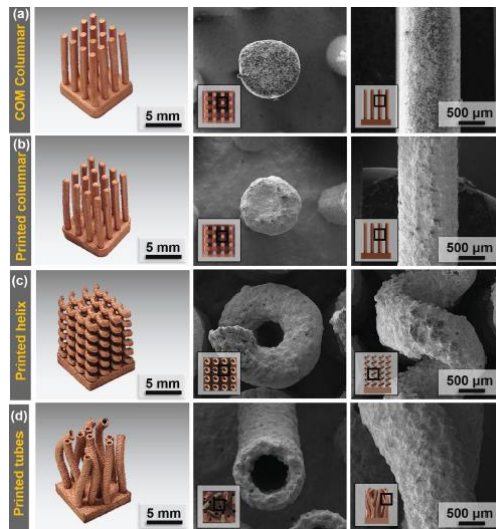


**Figure 6.** Top and side view photos (a) a commercial (COM) columnar, (b) a printed columnar, (c) a printed helix, and (d) a printed bent tubes heat sink [13].

In recent years, with the development of science and technology, some discontinuous laser heat sources which can be applied to SLM have appeared gradually. Kadena et al. [105] focused on SLM with discontinuous laser, which use the ultrashort laser pulses as a heat source. Through this study, it is found that the block metal produced by additive manufacturing with ultra-short pulse laser as a heat source is porous structure. This is due to the fact that there is no surface sintering in the production process but melting governs the process. Figure 7 shows the block images and SEM images produced by ultra-short pulse SLM during the experiment. It can be seen from Figure 7b that the results of the parts produced were unsatisfactory. Thus, this method is not suitable for making solid parts. Other thin-walled parts manufactured by this method are shown in Figure 7a,c. Although it seems that the molding effect of parts is not ideal at present, when manufacturing thin-walled parts with such complex structures, a larger aspect ratio can be achieved, which makes it suitable for future lightweight structures.

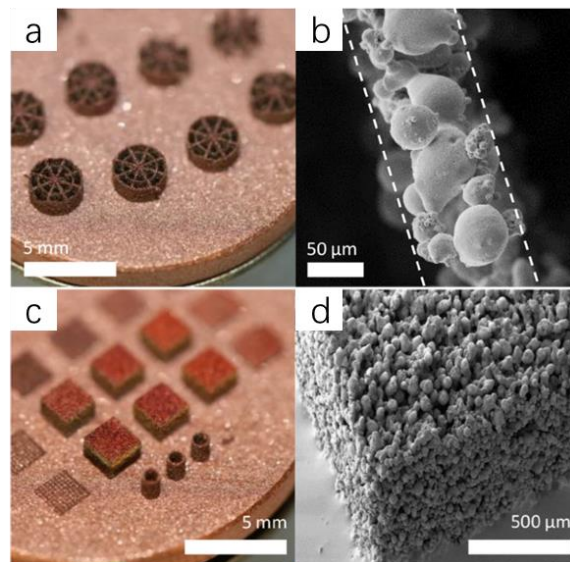


**Figure 7.** 3D image and SEM image of complex structures and block structure [105].

With the development of medicine, there is a growing need for artificial bones. In the review by Sing et al. [83], the research on the production of artificial bone by SLM and SEBM techniques is comprehensively described. They think additive manufacturing will have great potential in the production of artificial bones. The SEBM additive technology, which uses electron beam as heat source, has attracted a lot of researchers' attention

due to its unique advantages [98]. Compared with SLM additive technology, SEBM technology has a higher energy utilization ratio. The production of parts in a vacuum environment also makes the parts less susceptible to pollution. Moreover, the temperature is always kept at a high level during the production process, which reduces the temperature gradient during cooling and reduces the generation of internal stress [106]. Since SEBM technology was developed in 1997, the SEBM technology is used in different materials due to the increasing demand for complex structural parts [100]. For example, Schwerdtfeger et al. [76] studied the mechanical properties of Ti6Al4V periodic auxetic structure. Similar research has been done by Warmuth et al. [85], who concluded that the proper selection of the support amplitude is instructive for the change of deformation mechanism. Wolf et al. [74] studied the microstructure and mechanical properties of complex aluminum bronze parts produced by SEBM. With the development and innovation of a thermal manager, the production of pure copper complex components has also been put on the agenda, and the production of pure copper complex components by SEBM additive manufacturing technology has also attracted a lot of attention [104,107]. Ramirez et al. have published more than one paper [108]; they used SEBM technology to produce open-cellular copper structure and studied the microstructure and mechanical properties of the produced parts. Figure 8 shows the open cellular Cu sample produced by SEBM, and Figure 8 (1), (2), (4), and (6) shows the complex structure with stochastic mesh. Figure 8 (3), (5) shows the regular mesh structure. The slope of the Cu mesh structure is  $n = 2$ , while the slope of the random Cu foam is  $n = 2.4$ , which is consistent with the ideal opening foam slope of Gibson–Ashby foam model. The research also lays a foundation for the development of a pure copper heat exchanger. In the later research of Frigola et al. [49], complex pure copper parts were also produced through SEBM additive technology. In their research, it was found that  $\text{Cu}_2\text{O}$  in the parts would affect the physical properties of the parts. Although the existence of  $\text{Cu}_2\text{O}$  was also found in the study of Ramirez et al. [108] and it was confirmed that  $\text{Cu}_2\text{O}$  improved the mechanical properties of parts to a certain extent, it did not mention the impact on the physical properties of parts, while the study of Frigola et al. [49] filled in this gap.

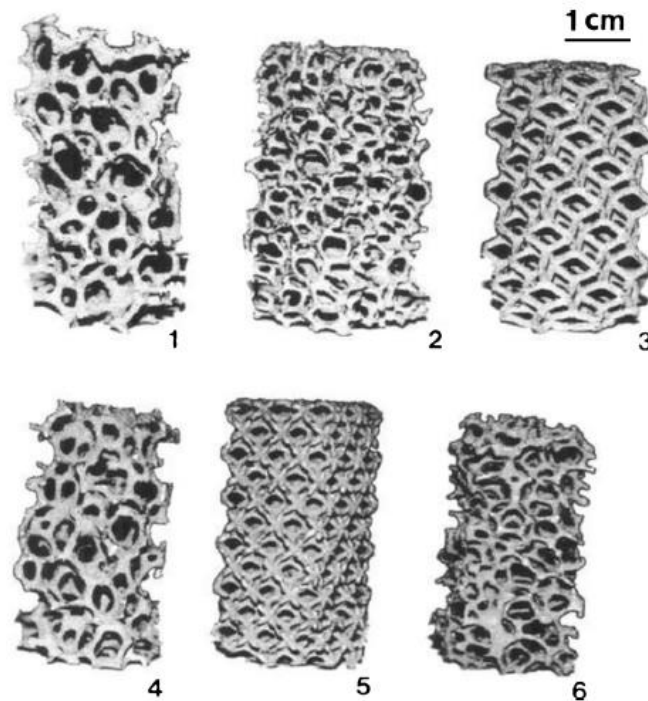


**Figure 8.** Examples of open cellular Cu mesh and foam specimens [108].

It is difficult to find the defects in additive manufacturing of complex components. These defects will affect the performance and service life of the parts, and it is difficult to detect the existence of defects with traditional nondestructive evaluation techniques [6]. Ledford et al. [87] provided a new method for artificial monitoring of the SEBM additive process. They monitored the additive process using in situ real time backscatter electron monitoring. After detection, it is found that the real-time monitoring results are highly consistent with the real results. When this technology is combined with parts processing, it will provide good feedback for mass processing. In recent years, the application of pure copper additive manufacturing in industrial production had

been put on the agenda, and the feasibility of SEBM additive technology in industrial production was discussed in the research of Urena et al. [109].

One of the studies in 2009 proposed to use additive manufacturing to produce complex-shaped heat exchangers, and to promote the development of the industry. Researchers have explored different additive manufacturing technologies. The feasibility of BJ additive technology in the production of pure copper parts was explored in the research of Bai et al. [96]. In this paper, it is pointed out that the research on the production of pure copper by BJ technology should focus on improving the density of sintered parts. Although BJ additive manufacturing technology does not produce greater internal stress than PBF additive manufacturing technology due to low processing temperature, and is more suitable for the production of pure copper parts, there are still some problems in processing [110]. Miyanaji et al. [88] studied the influence of the raw powder material, print head and the interaction between binder and powder bed on part forming, and proposed how to produce a qualified pure copper part by controlling these conditions and using BJ additive technology. In addition, the parts produced by BJ additive manufacturing technology need post-processing. It is also mentioned in the paper that if you want to produce a qualified part, the coupling of post-processing technology and production parameters should be considered. When using BJ additive technology to produce parts, it is inevitable that the parts will not be compact enough, which will be challenged by defects. Some scholars reduce the occurrence of defects by adjusting process parameters and other methods, while some scholars use defects to produce parts with foam structure. In the study of Miyanaji et al. [111], the foam structure of pure copper was produced by BJ additive manufacturing. Figure 9 shows the pure copper foam structural parts produced during the experiment. It is found that after annealing at 600 °C for 2 h, the final porosity can reach up to 59% and the volume shrinkage rate is the lowest (5%). This is contrary to the traditional idea of increasing density, but the disadvantages of BJ additive technology are turned into advantages and given full play.

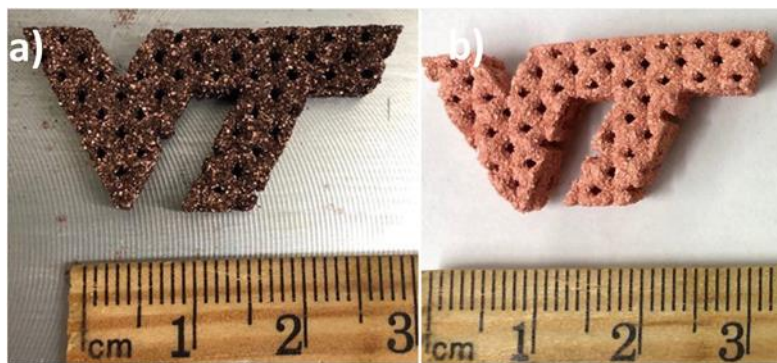


**Figure 9.** Copper foam part fabricated via AERO-Binder Jetting (a) green part (b) after sintering and annealing [102].

## 3.2. Shaping Property

### 3.2.1. Forming Properties of Parts Manufactured by SLM

The density is an important indicator for judging the formation of samples [112]. At present, most of the studies on pure copper additive manufacturing are still seeking to solve the problem of low density. Due to the high reflectivity of pure copper to laser [2]. In the previous study by Syed-Khaja A et al. [113], it was also mentioned that there are challenges in applying pure copper to SLM additive manufacturing, but there are also had great application prospects. The research of Sciammarella et al. [114] also mentioned the application prospect of copper, such as the research of Whirlpool that the use of copper components can reduce cycle time by 20% and warpage by more than 50%.

Figure 10 shows the relationship of laser power, energy density and relative density of pure copper part manufactured via SLM additive manufacturing in recent years. The formula for calculating energy density is that:

$$E_b = \frac{P}{v d h} \quad )$$

where  $E_b$  is the energy density,  $P$  is the laser power,  $v$  is the scanning speed,  $d$  is the hatch distance, and  $h$  is the powder thickness.

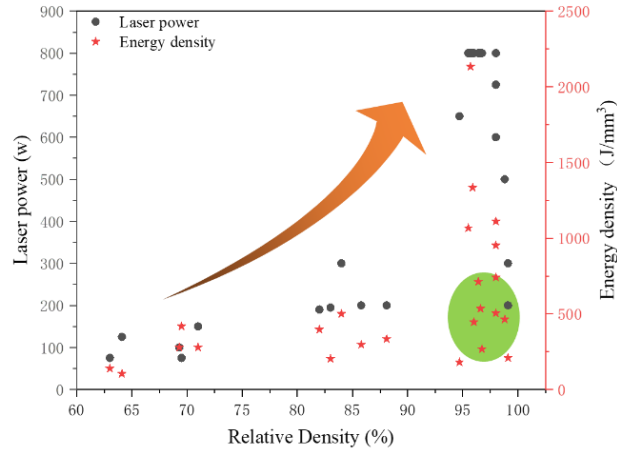


**Figure 10.** The relationship between laser power and relative density of pure copper part manufactured via SLM additive manufacturing [1,2,5,7,9,10,27,37,39,40,42,43,45].

As can be seen from the figure, when the power is less than 300 W, the relative density of parts produced by SLM is difficult to meet the industrial use standard. The laser power and the relative density of the part show a positive correlation trend. The phenomenon is due to the high reflectivity and high thermal conductivity of pure copper. Nowadays, the most widely used laser wavelength range is 1000–1100 nm. The pure copper powder has a reflectivity of 71–72% to this wavelength range laser [27]. In the early years of commercial SLM equipment, the maximum power was generally less than 200 W [10], so the relatively high density of formed parts was rarely produced in the study of pure copper at that time [40]. In addition, it can be seen from Figure 10 that when the energy density is concentrated in the region of 250–750 J/mm<sup>3</sup> (the green region in Figure 10), combined with high power, parts with relatively high density could be obtained. In the research of Jadhav et al. [39] also confirmed that it is easier to get denser formed parts under high laser power. Although SLM devices do not provide higher power output, researchers have found a way to increase the relative density of parts. Some scholars make up for the shortcomings of insufficient heat by preheating the substrate, and others use different wavelengths lasers to increase the powder's absorption rate of the laser. In the study of Pavel Lykov et al. [44], it was found that when the substrate was preheated at 140 °C, the porosity inside the parts decreased from 3% to 0.88%. In the study by Trevisan F et al. [5], a laser power of 200 w was also used and the substrate was preheated at 100°C. The finally formed parts with a relative density of 83% were obtained. In the research of HongZe Wang et al. [72], a SLM device based on blue laser (445 nm) was developed for the first time. It was found that the absorptivity of the steel powder to the blue laser was 2.5 times than the laser of wavelength range is 1000–1100 nm. This technology also provides a new method for pure copper SLM. Although the density of these parts has been greatly improved, it is still difficult to reach industrial standards. In addition to changing the wavelength of the laser, Zhang DQ et al. [45] improved the spot of the laser and transformed the traditional Gaussian heat source into a uniformly distributed heat source. Compared with the Gaussian source, the uniformly distributed laser beam can reduce the energy loss in the additive manufacturing process and reduce the occurrence of defects. With the advancement of technology, the SLM equipment had been continuously upgraded and had the ability to produce parts with high power. Some researchers even assemble individual modules to build high-power SLM equipment. For example, In the study of Matteo Colopi et al., they built a 1 kW single-mode SLM system. Through a large number of experiments, they found that the samples produced by high-power single-mode laser were well formed and the density could meet the requirements. In the paper of “Selective laser melting of pure Cu with a 1 kW single mode fiber laser”, they determined the range of acceptable parameters after a large number of experiments [8,43]. As shown in Figure 11, the portion of the blue dotted box is the area of acceptable parameters for SLM of pure Cu indicated. The parts produced in this area are shown in Figure 11, in which macro picture is on the left and optical microscopy picture is on the right. The density of the parts within this acceptable machining area is measured at over 97%.



**Figure 11.** (a) Qualitative categorization of process outcome; (b) Final demonstrator produced by pure copper powder [43].

However, the laser power is not as high as possible. When the power is too high, it will also cause defects. In the study of Jie Yin et al. [49], they found that when the high-power additive was used, the molten pool would become unstable and spatter would form. This conclusion is similar to the experimental result of Colopi M et al. [43]. In the study of Ken IMAI et al. [37], it was also found that when the power is too high, the laser forms a keyhole in the molten pool. The keyhole is not stable during the laser advancement process, which causes spatter and internal defects of the parts. It can be seen that the stability of the molten pool is a key factor affecting the forming of parts [115]. In the process of SLM additive manufacturing, the way of heat transfer in the molten pool determines the stability of the molten pool [30,57]. The schematic diagram of heat transfer in the SLM process is shown in Figure 12. Figure 12a shows the heat transfer in the laser molten pool during the SLM process, and Figure 12b shows the simplified mathematical model of the laser molten pool. As shown in Figure 12a, in the SLM additive process, the heat from the laser is not 100% absorbed, but released through convection, radiation and evaporation. According to the research, the heat loss is about 20% of the total energy input [9].

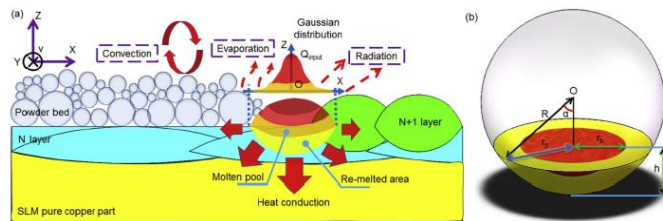


**Figure 12.** Schematics of heat transfer process of a molten pool during SLM processing [9].

In the study of L. Constantina et al. [13], the stability of the molten pool under different heat input conditions was verified. It can be seen from Figure 13 that the surface forming of parts is different when different scanning speeds are adopted. When the scanning speed is 200 mm/s, the surface tension of the molten pool is greatly different due to the large temperature gradient inside the molten pool. As a result, the molten pool flows toward the middle, resulting in the defects of curling. When the scanning speed is 400 mm/s, the molten pool is stable and the parts are well-formed. When the scanning speed is increased to 600 mm/s, it is difficult to maintain a stable molten pool due to insufficient energy, so porous parts are produced.

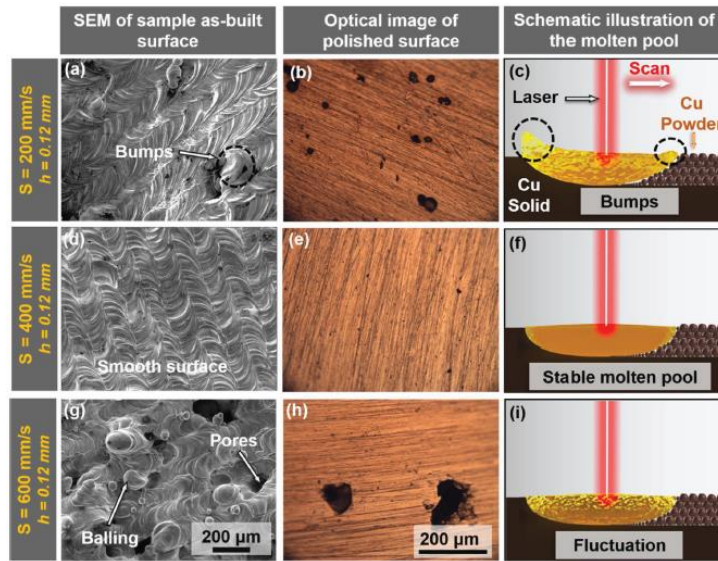


**Figure 13.** (a,d,g) SEM micrographs of as-built surface sand (b,e,h) optical images of polished surfaces with scan speeds of 200, 400, and 600 mm/s, respectively, and (c,f,i) schematic illustrations of the molten pool shapes at different laser scan speeds [13].

In addition, not only the laser power has the influence on the forming of parts, there are also some factors in the production process that will affect the forming of parts. In the study of Matteo Colopi et al. [8], it is found that different substrates have an impact on the forming of parts. By using the same process parameters to compare the parts manufactured on different substrates, it was found that the parts manufactured on the substrates with low thermal conductivity have higher density. By comparing the steel, copper and steel-copper substrates, they found that the parts added on the steel plate have a higher density, and it is proved that the substrate with high scanning speed and low thermal conductivity needs to be matched under the condition of high power. Under the above conditions, the part density is up to  $99.1\% \pm 0.2\%$  with a build rate of  $12.6 \text{ cm}^3/\text{h}$ . This conclusion is also supported by the work of Siva Prasad H [71] and Sciammarella F et al. [114]. In their study, it was believed that the deficiency would be caused by insufficient heat input when SLM additive is used to produce pure copper. The high thermal conductivity of the substrate will accelerate the heat loss and make it difficult to form the parts. The purpose of using a low thermal conductivity substrate is also similar to preheating the substrate of SLM additive fabrication with a low-power laser in earlier studies. In the study by Ikeshoji TT et al. [2], the influence of different hatch distance on shaping was studied. In their initial speculation, they thought that the smaller hatch distance would melt the splash and bulge. However, in the follow-up observation, it was found that small hatch distance could not reduce the impact of these defects but would continuously aggravate the occurrence of defects. When the hatch distance is too large, the effective overlap will be insufficient. It is difficult to melt all the powders and cause defects. Figure 14 was shown the positions of different hatch distances from the edge of the weld pool in the x direction. It could be clearly seen that when the hatch distance is 0.1 mm, the molten pool was the most stable, and the relative density of 96.6% part was obtained.

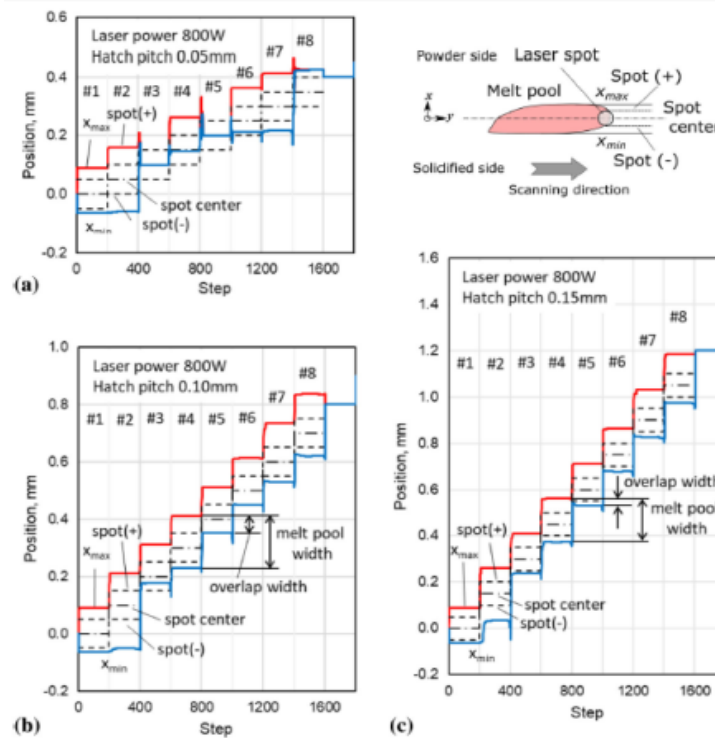


**Figure 14.** Positions of melt pool rim in x-direction (width) for hatch pitch of (a) 0.05 mm, (b) 0.10 mm, and (c) 0.15 mm [2].

### 3.2.2. Forming Properties of Parts Manufactured by SEBM

The way of SEBM additive manufacturing is different from SLM additive manufacturing, the key research direction of SEBM additive manufacturing is not to increase the relative density. Using SEBM additive manufacturing can easily obtain formed parts with a relative density of more than 99% [49]. This is due to the fact that the pure copper powder is much less reflective to the electron beam than the laser beam, and can provide higher heat input under the conditions of SEBM additive manufacturing [28,84]. For example, in the study of Guschlbauer R et al. [4], only 275 W energy input was used to obtain parts with a relative density greater than 99.5%. However, due to the difficulty of heat dissipation, the cooling time of parts produced by SEBM additive manufacturing conditions is too long, which is prone to element segregation and defects. In the study of Soroush Momeni et al. [116], copper-chromium alloy powder was used for SEBM additive manufacturing. It is found that there are chrome-rich spheres ( $<1 \mu\text{m}$ ) embedded by Cu matrix in the microstructure of formed parts. In the manufacturing process of SEBM additive, the oxidation of pure copper powder due to storage and other reasons cannot be ignored, and the presence of oxide has a great influence on the forming of parts. For this reason, many researchers have done related research on the influence of oxygen on the performance of parts. R Guschlbauer et al. [28] studied the effect of oxygen on part performance during SEBM production. The authors used two batches of pure copper powder, one of which had higher oxygen content ( $0.0545 \pm 0.0009 \text{ wt\%}$ ). Figure 15a shows the distribution diagram of the forming status of high-oxygen powder under different process parameters when the substrate is preheated to  $530 \text{ }^\circ\text{C}$ . It can be seen from the figure that when the scanning velocity was less than  $1 \text{ m/s}$ , the sample appeared cracks, and when the scanning velocity was between  $1\text{--}1.5 \text{ m/s}$ , the sample was basically not formed. Figure 15b–d shows the distribution diagram of copper oxide for two powders produced under SEBM. The scanning speed and power used are  $0.5 \text{ m/s}$  and  $450 \text{ W}$ , respectively. Figure 15b,c shows the distribution diagram of CuO with cracked parts produced by high-oxygen powder processing, and Figure 15d shows the distribution diagram of  $\text{Cu}_2\text{O}$  produced by powder processing with low oxygen content. It can be seen from the figure that  $\text{Cu}_2\text{O}$  distribution in parts produced by powder with high oxygen content is regular, and the content of  $\text{Cu}_2\text{O}$  is high. In the research of Lodes MA et al. [47], it is found that to a certain extent, the scanning speed has little effect on the forming of parts produced by SEBM technology, but cooling is the key factor. Their research results show that lower processing temperatures are required when producing large part, and a certain amount of cooling time needs to be added if necessary.

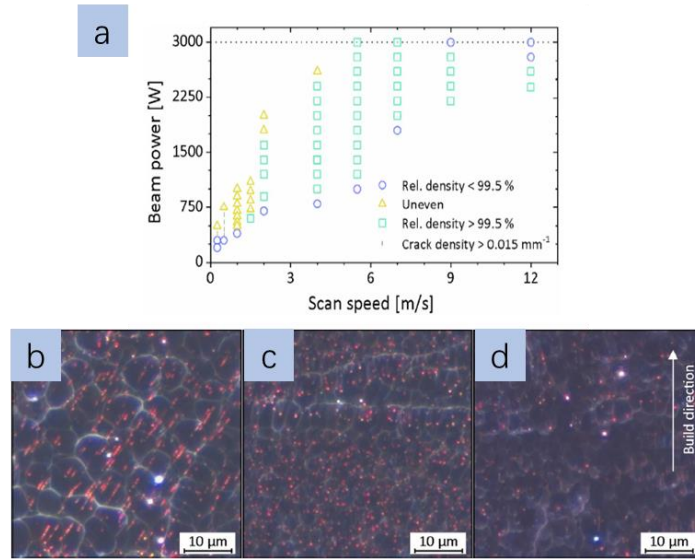


**Figure 15.** (a) High oxygen content powder at a process temperature of 530 °C; (b–d) Light microscope pictures in dark-field mode showing the Cu<sub>2</sub>O distribution. (b,c): set II with cracks, (d): set I without cracks [28].

In order to minimize the influence of oxides, Christopher Ledford et al. [6] used a hydrogen furnace to process the pure copper powder and then performed the SEBM additive experiment to determine the oxygen-scavenging ability of this method. To determine the oxygen scavenging ability of hydrogen furnace powder, the authors prepared three powders with different oxygen content, namely low oxygen content, medium oxygen content and high oxygen content pure copper powder. When the three powders were treated in a hydrogen furnace, hydrogen was added to the powder and part of the oxygen was consumed. The hydrogen heat treated and untreated hydrogen and oxygen content pairs of the three powders are shown in Table 2. After the powder is treated, the experiment is carried out as shown in Figure 16. Figure 16a shows the equipment required for the experiment. Two types of equipment residual gas analysis and IR camera were added to the vacuum chamber of the SEBM equipment, and two-color pyrometer and thermocouple were used to monitor the temperature of the surface. In the experiment the researchers used different kinds of powder to deposit a layer of pure copper under the action of an electron beam. The H<sub>2</sub>O released from the melt pool will be detected by residual gas analysis. It was found that the powder after hydrogen heat treatment was suitable for SEBM, and this method could effectively remove oxygen elements, thus reducing the influence of oxide on the mechanical properties of SEBM parts. Measurements of oxygen elements in the sedimentary layer showed that the oxygen content in the pure copper parts made by SEBM was only 50 wt. ppm. In order to avoid the influence of H<sub>2</sub>O on parts, the authors also studied and measured it. They found that the H<sub>2</sub>O could escape from the heat-affected zone and molten pool during the process of SEBM, and when the multilayer parts were deposited would provide sufficient time for H<sub>2</sub>O to overflow.

**Table 2.** Chemical content of copper powders [6].

Powder ID	Condition	Average O <sub>2</sub> (wt. ppm)	Standard Deviation (wt. ppm)	Average H <sub>2</sub> (wt. ppm)	Standard Deviation (wt. ppm)
LO-Cu (15–53 μm)	Untreated	226.51	11.36	0.87	0.56
	Hydrogen Treated	54.76	8.34	1.56	0.97
LO-Cu (15–53 μm)	Untreated	462.17	18.87	1.81	0.66
	Hydrogen Treated	282.33	3.79	31.83	2.02
LO-Cu (15–53 μm)	Untreated	1507.33	12.70	1.95	0.99
	Hydrogen Treated	586.97	35.28	76.44	5.77

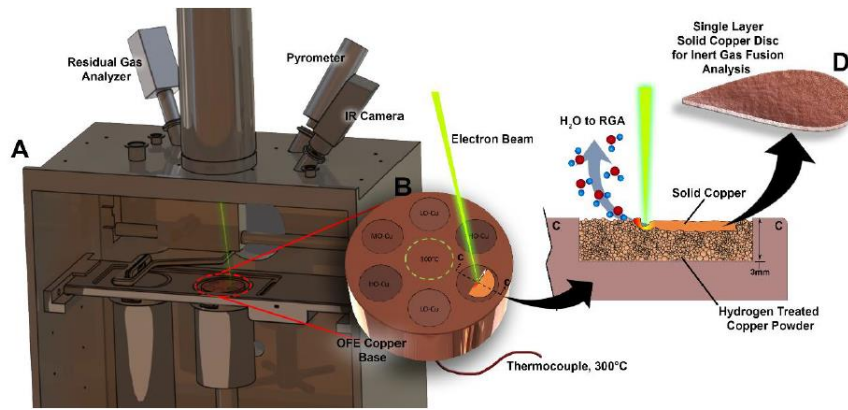


**Figure 16.** Description of in-situ H<sub>2</sub>O vapor outgassing experiment [6].

### 3.2.3. Forming Properties of Parts Manufactured by BJ

Compared with PBF additive manufacturing, BJ additive manufacturing is a unique method. Although the applicable material types are less limited, it also brings some problems [97]. The application of binder and heat treatment in the process of manufacturing parts, the internal parts are easy to produce holes and other defects [95]. In order to reduce the influence of porosity, A.Y. Kumar et al. [110] have performed related research. They used hot isostatic pressure to reduce the porosity of the parts. The powders used in the experiment were mixed with a median particle diameter of 30  $\mu\text{m}$  and 5  $\mu\text{m}$  at a ratio of 73:27 by weight. The comparison of section porosity between the parts treated by hot isostatic pressure and the parts not treated is shown in Figure 17. According to the image analysis, the porosity of the untreated parts is 1.88% (as shown in Figure 17a), and of the treated parts is only 0.13% (as shown in Figure 17b). In addition, they found that the parts treated with hot isostatic pressure produced anisotropic shrinkage due to graded density in the green part.

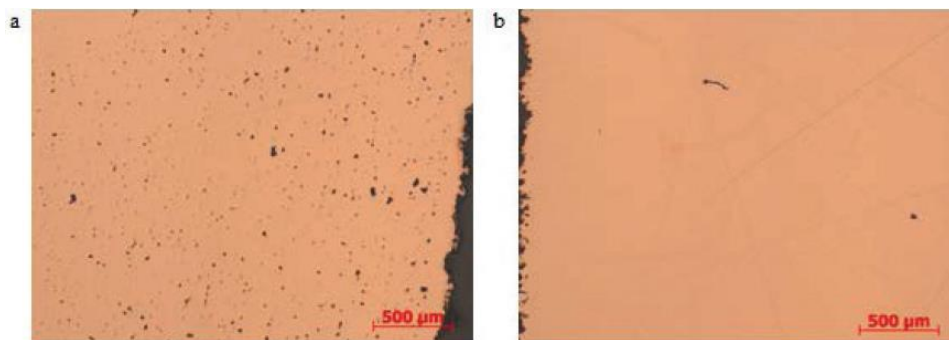


**Figure 17.** Sample micrographs indicating density improvement upon HIP [110].

This result is similar to another study by A.Y. Kumara et al. [50], which investigated the effect of process-induced porosity on material properties of parts produced with BJ technology. Three types of pure copper powders were used in their research, 17  $\mu\text{m}$ , 25  $\mu\text{m}$  and mixed powders (particle size of 30  $\mu\text{m}$ , 5  $\mu\text{m}$  mixed in a ratio of 73:27). All parts are produced in two copies, one of which is treated with hot isostatic pressure to obtain high density parts. Figure 18 is a schematic diagram of performance comparison for the parts. From the trend of the lines in the figure, it can be seen that the high density parts have higher tensile strength and thermal conductivity. This trend is the same as that predicted by the author in the paper. From their study, it can be seen that the mixed powder has higher density and better performance.

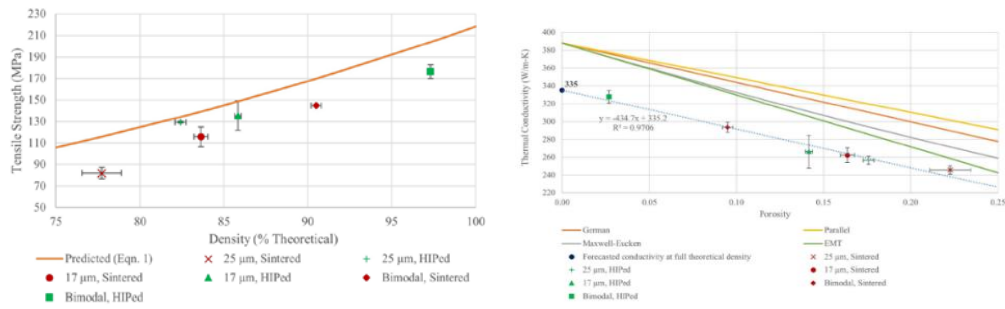


**Figure 18.** Performance comparison of different parts [50].

Yun Bai et al. [117] studied the influence of powder particle size distribution on powder packing and sintering during parts production with BJ additive manufacturing technology. Compared with the traditional single powder production parts, the use of bimodal powder mixtures can improve the powder fluidity and significantly reduce the porosity and shrinkage of the formed parts. By testing the forming parts, compared with single powder, the bimodal powder mixtures can improve 8.2% powder's packing density, 10.5% fluidity and 4% sintering density. At the same time, the sintering shrinkage rate was reduced by 6.4%. In an earlier study by the authors, the role of bimodal powder mixtures in promoting the forming of parts was discussed. It has also been verified that expanding the particle size distribution through the bimodal powder mixtures without changing the median particle size is a feasible strategy. The parts will shrinkage after sintered, which is caused by the loss of the binder and the looseness of the green parts [118]. In order to improve the forming density of parts, Yun Bai et al. [119] used inkjetted nanoparticles instead of binder and analyzed the parts produced by BJ additive manufacturing technology. During sintering stage, the nanoparticles melt to form stable connections that enhance the strength of the parts. According to the sintering conditions, the sintering density can be increased by 12.3% [94]. When faced with some processing that requires the accuracy of parts, the method of BJ additive manufacturing should be consider carefully.

### 3.2.4. Measurement and Improvement of Forming Properties

With the continuous development of additive manufacturing technology, in order to better determine the relative density of parts, Santo L et al. [42] developed a new method of measuring the relative density of parts. In the experiment, they prepared five sets of parts with relative density between 63% and 71%. The pressure test is carried out on the surface of the polished part by using the tungsten carbide pressure head with a diameter of 1 mm, and the indentation size is the same and the pressure is recorded. The test results show that the instrument indentation method can effectively measure the density of parts in the local range, and it is found that there is a linear relationship between the indentation pressure and the density of samples. Faced with the production of some parts with higher surface quality requirements, it is difficult for the formed parts to directly reach the use standard, so special methods are needed to treat the surface of the parts [73,120]. In the study by Karakut I et al. [121], a method called magnetically driven abrasive polishing technique was developed. This method can be used to polish the surface of complex parts. Figure 19 shows the schematic diagram of this method. In this process, an abrasive mixture of magnetic and abrasive particles is used in a viscous liquid, and magnetic particles are attracted by an oscillating external magnetic field, causing these particles to move in sync with the magnetic field, thus achieving a polishing effect. After testing the surface roughness of the parts, it is found that the surface roughness has been greatly improved, from an average surface roughness of about 35 μm to 4 μm.

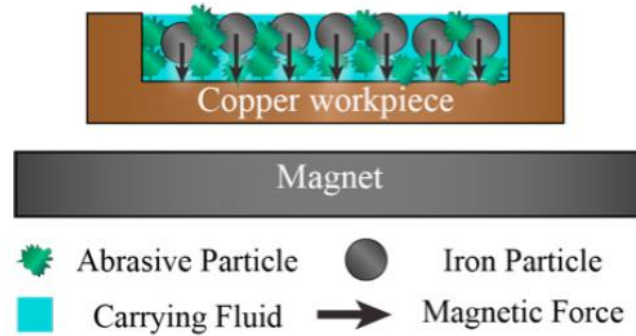


**Figure 19.** Performance comparison of different parts [121].

### 3.3. Mechanical and Physical Properties

#### 3.3.1. Mechanical Properties

The mechanical and physical properties of pure copper parts are closely related to density. In general, high-density parts have better mechanical and physical properties [38]. In the following part, the research on SLM, SEBM and BJ technology will be reviewed to analyze the factors affecting mechanical and physical properties.

In the study of Jadhav SD et al. [7], pure copper parts with a relative density of 98.8% were processed by SLM additive manufacturing. After testing the mechanical properties, it is found that the tensile strength of the part is 270 MPa and the microhardness is 93 HV. In the study of Lykov PA et al. [10], SLM additive manufacturing technology was also used to produce pure copper parts with a relative density of 88.1%. After testing, it was found that the tensile strength of the parts was 149 MPa. Guan J et al. [40] produced parts with SLM additive manufacturing technology with a relative density of 82% and a microhardness of 61.48 HV. This shows that the mechanical properties of the parts are seriously affected by the relative density. In the study of Guschlbauer R et al. [4], they produced parts with a relative density of more than 99.5% through SEBM additive manufacturing technology. After the mechanical property test, it was found that the maximum tensile strength of the parts was 177 MPa and the maximum hardness was 57.8 HV, but the mechanical property was less than the pure copper parts produced by Jadhav SD et al. [7]. This is due to the higher temperature in the process of producing parts under the SEBM technology, which makes the internal microstructure of the parts coarser [95,98]. Their research found that the oxide has a promoting effect on the absorption of laser, and played a certain strengthening effect. Compared with SLM technology and SEBM technology, the mechanical properties of samples produced via BJ technology are significantly lower, because the parts produced by BJ technology are less dense. In the study of Ashwath Yegyan Kumar et al. [50], they obtained a sample with the highest density of 83.6%, and the tensile strength obtained after the tensile test was 115.8 MPa. Compared with the study of Guan J et al. [40], the tensile strength is higher. This is because the influence of internal stress is greatly reduced due to the heat preservation process in the powder sintering process, while the SLM technology is due to It is a rapid cooling process, so the internal stress existing in the low-density parts will reduce the mechanical properties of the sample.

The first method of improving the mechanical properties of parts produced by SLM technology is to improve the relative density of parts. In the study by SD Jadhav et al. [1], the innovative addition of carbon nanoparticle to pure copper powder was used to increase the powder's laser absorption rate and improve the relative density of parts. It was found that the fluidity and laser absorption of copper powder were significantly enhanced after the addition of 0.1 wt % carbon nanoparticles. At low laser energy density (200–500 J/mm<sup>3</sup>), the finished metal blocks with a density of more than 98% were finally produced. The highest density of parts is produced when the laser power is 725 W. The addition of carbon nanoparticles not only improves the laser absorption of pure copper powder, but also reduces the influence of oxygen on the performance due to in-situ de-oxidation of carbon. However, the test results of mechanical properties were unsatisfactory, the maximum tensile strength was only 125 MPa. After the analysis of the fracture, they believed that the defects were mainly caused by segregation of elements such as carbon, phosphorus and oxygen, which reduced the mechanical properties. In terms of improving density, BJ technology is different from traditional PBF technology. The density of formed parts is generally affected by the sintering process. In the research of Gurminder Singh et al. [51], the density of parts is often improved by controlling the parameters of the sintering process. They found that

sintering temperature and holding time are negatively correlated with porosity (with the increase in sintering temperature, porosity: 24.78–6.08%; with the extension of holding time, porosity: 12.3–7.39%), The heating rate is positively correlated with the porosity (as the heating rate increases, the porosity: 6.08–17.36%). In addition, in their research, it was found that ultrasonic-assisted sintering can effectively improve the tensile strength of parts. The research results show that compared with traditional sintering process using ultrasonic-assisted sintering, the tensile strength of parts is increased 15–45%.

The parts produced by SEBM can obtain high relative density parts when the parameters are suitable. In the study of Guschlbauer R et al. [4], it was found that when the energy density of the electron beam is too high, the parts will have a greater tendency to crack. They believe that on the one hand, the high oxygen content at the grain boundaries causes brittle intergranular cracks. On the other hand, the internal stress generated by the experimental device caused cracks to form. Besides, most scholars are looking for ways to strengthen the performance of the parts on this basis. Pobel CR et al. [21] studied the dispersion strengthening of oxide at SEBM pure copper. They added 2.28 wt%  $\text{Al}_2\text{O}_3$  to the pure copper powder. As shown in Figure 20, after microstructural analysis of the produced block, it is found that there are three phases inside the block, which are marked in Figure 20b,c. After EDX detection, these three phases are: pure copper phase (marked as 1 in Figure 20b); The phase containing Cu, Al and O is composed of ceramic phases dispersed in the copper matrix (marked as 2 in Figure 20b). The second phase, which consists of pure aluminum (marked 3 in Figure 20c). It is found that the strengthening phase can improve the performance of the part. Although the separation of alumina from copper can be reduced by decrease the preheating temperature. It is difficult to make the second phase not occur inside the part. In their experiments, they found that the forming of parts was acceptable, but the inside was full of defects such as pores. Therefore, the oxygen content in raw materials should be minimized when making pure copper parts via SEBM. Great efforts have also been made to address the effects of oxides in raw materials on the performance of part.

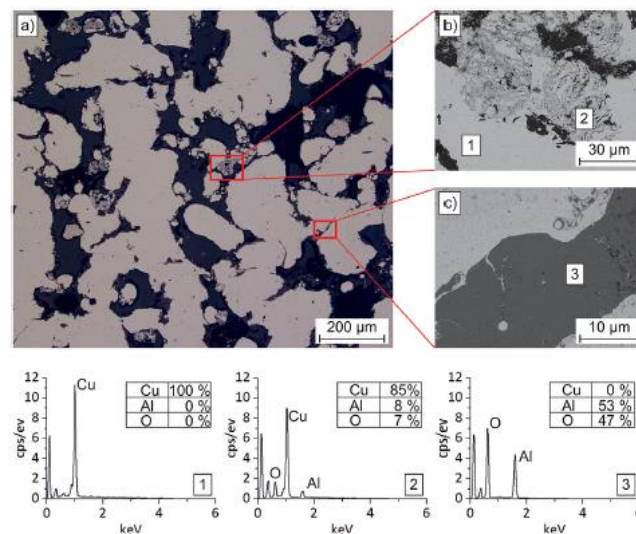


Figure 20. Microstructure of ODS-Cu processed via SEBM [21].

However, the presence of oxide does not always play a bad role. In the study of Ramirez DA et al. [48], a new precipitate–dislocation architectures was found under the influence of  $\text{Cu}_2\text{O}$ . This architecture has high hardness and has the function of enhancing the performance of parts. When this structure exists, the hardness range of the parts is increased to 83–88 HV. Compared with the copper substrate, the microhardness of the parts with this structure has increased by 54%. The research of Guschlbauer R et al. [28] further determined the influence of oxides on the performance of parts. They used two kinds of powders with different oxygen content to test and found that the presence of a small amount of oxides should enhance the performance of parts. If the content is too high, it will cause internal defects in the part. Unfortunately, the article does not give the oxygen content in which range can enhance the performance of the part.

### 3.3.2. Physical Properties

The excellent physical properties determine the broad development prospect of pure copper parts [4,43]. In the research of S.J. Raab et al. [38], they found that the thermal conductivity and electrical conductivity are

seriously affected by the relative density of the pure copper parts. In the research, they produced pure copper parts with a relative density of 99.95% through SEBM. Through the test of electrical conductivity and thermal conductivity, it is found that the electrical conductivity of the part is 96.24% International Annealed Copper Standard (IACS), and the thermal conductivity is 400.1 W/m·K. They also found that the electrical conductivity and thermal conductivity follow the Wiedemann-Franz law. As shown in Figure 21, it is the relationship between electrical conductivity, thermal conductivity and relative density. From the distribution of points in the figure, it can be seen that when the relative density of the part is greater than 99%, the physical performance is improved greatly [1,4,7,27,38,39,49]. This is consistent with the conclusion obtained by S.J. Raab et al. [38] that the higher the relative density, the better the physical properties. In their study, they also suggested that the presence of phosphorus in the forming parts can affect the electrical conductivity and thermal conductivity of the parts. This is similar to the results of S.D. Jadhav et al. [1], where parts are produced via SLM. Even though the relative density of the tested parts was 98%, the electrical conductivity was only 39% IACS, far below the average level. When the researchers examined the fracture, they found carbon and phosphorus accumulating in the defect. It has been confirmed that phosphorus is the main reason for the low electrical conductivity of the sample, thus proving that the choice of raw materials on the performance of the parts is also particularly important. The research of R. Guschlbauer et al. [4] also proved this point. The physical properties of pure copper parts produced by SEBM using different purity powders are different. The parts produced by using high-purity powders have fewer defects and less segregation. This view also applies to parts produced by BJ technology. In the study of Yegyan Kumar et al. [50], the density of parts produced by using bimodal powder after hot isostatic pressing reached 97.3%, and its conductivity reached 93.6% IACS. They study that there is still room for further improvement in electrical conductivity, because the binder produces carbides and oxides after thermal decomposition. These impurities accumulate at the grain boundaries, thereby reducing the conductivity. The thermal conductivity obtained in their research is 327.9 W/m·K. This is similar to the results of Gurminder Singh et al. [51]. The thermal conductivity of parts produced by Gurminder Singh et al. using BJ is 338.14 W/m·K when the density is 93.92%.

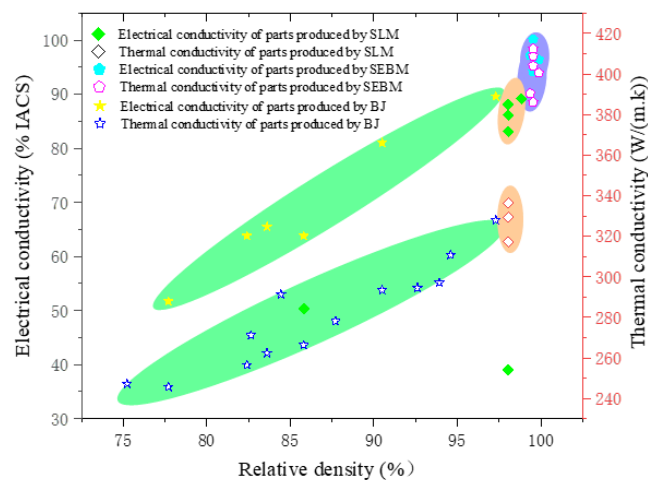


**Figure 21.** The relationship between electrical conductivity, thermal conductivity and relative density [1,4,7,27,38,39,49–51].

In addition, C. Silbernagel et al. [27] also mentioned in their research that the crystal structure also has a great impact on the physical properties of the parts. They use SLM to produce parts with a relative density of 85.8%. Then the resistivity was measured in the directions perpendicular to the substrate, parallel to the substrate and at an angle of 45°. The maximum resistivity was found in the direction perpendicular to the substrate, 24% higher than the average resistivity in the other two directions. They believed that the difference of resistivity of different orientations was mainly caused by the difference of interlayer and defects in interlayer caused by unmelted powder particles. Besides, S.D. Jadhava et al. [39] studied the influence of SLM process parameters on the texture evolution of pure copper. Due to the rotation of the scanning angle of each layer by 90°, a unique texture was produced and the conductivity of the sample reached 88% IACS.

---

#### 4. Prospect and Challenge of 3D Printing in Pure Copper

Pure copper is widely used in electric power, heat dissipation, pipelines, decoration and other fields due to their excellent electrical conductivity, thermal conductivity, corrosion resistance and toughness [122]. Some copper alloy materials have good electrical conductivity, thermal conductivity and relatively with high strength, it is widely used in the manufacture of electronic, aviation and aerospace engine combustion chamber components [16]. Nowadays, we are facing the challenge of lightweight and structural complexity in the industry. The method of additive manufacturing can solve these problems well [100].

In order to ensure the performance and availability of parts in the actual production, the appropriate additive manufacturing method should be selected [19]. The parts produced by SLM have high precision, but the reflectivity of copper is high, and the adaptability of process parameters is high. In addition, due to the fast heating and fast cooling of SLM processing method, it is easy to produce large internal stress inside the sample. Although the influence of internal stress can be reduced by substrate preheating and post-processing, it also increases the complexity of the process [100]. SEBM technology is a more suitable method for pure copper additive, but at the same time, due to the high equipment price limits the wide application of this technology, the accuracy of the production parts is also slightly lower than SLM technology [95]. The BJ technology can produce green parts at low energy density, it must be reprocessed. Compared with SLM and SEBM technology, BJ technology is difficult to ensure the accuracy of parts during post-processing, and the parameters in the sintering process also have a great influence on the forming of parts [94].

In the study of pure copper parts, researchers have made great efforts. In addition to the SLM, SEBM and BJ technologies mentioned in this article, many researchers have explored other methods of producing complex pure copper parts, such as SLS [24], UAM [123], LMD [122] technology, etc. The technologies like SLS and BJ are known as two-step processes, through printing to get green body, and then through post-processed in a separate operation or sintering to achieve full density [124]. SLS technology originated in the 1980s. Nowadays, the technology has become a research hotspot, and is gradually applied in industrial production [125]. F.L. Amorim et al. [126] Studied the EDM electrodes performance difference between the copper alloy material and the pure copper material via SLS technology. This study provided a new idea for the industry. Although the final conclusion found that the effect was not ideal, the EDM electrode made by pure copper via SLS could not achieve good working effect due to the large number of holes inside the parts, which also pointed out the direction for future research. The UAM additive manufacturing technology is different from SLM and SEBM additive manufacturing technology. In the process of UAM additive manufacturing, no heat source is required [36,123,127]. A small part of the heat in UAM technology is generated by friction, so most scholars prefer to use diffusion bonding and friction stir welding to compare with UAM [127,128]. It is believed that the bonding mechanism of UAM additive manufacturing technology is the stick-slip motion between two foils. This bonding mechanism lies between the bonding mechanism of diffusion bonding and friction stir welding [36,127,129]. Due to the low power of commercial UAM additive manufacturing equipment, it is only suitable for processing some materials such as thin aluminum. Therefore, Edison Welding Institute developed a high-power UAM additive manufacturing technology, namely "very high power ultrasonic additive manufacturing" (VHP UAM) [31,131]. This also provides a new method and idea for UAM additive manufacturing of pure copper. In the study of M.R. Sriraman et al. [132], the binding characteristics of pure copper VHP- UAM additive manufacturing were studied. In this experiment, 150  $\mu\text{m}$  copper foil was used as raw material for VHP-UAM additive manufacturing. The hardness test of the parts showed that there was obvious softening and enhanced plastic flow in the production process. The grain size of the raw material was 25  $\mu\text{m}$  before processing, and a dynamic recrystallization zone of 0.3–1.0  $\mu\text{m}$  was formed at the interface after short processing. This phenomenon causes metallurgical bonding to migrate through grain boundaries and allows continuous welding of the tape to form three-dimensional sections. At present, there are not many studies on UAM additive technology for making copper complex parts. On the one hand, it is limited by the technology itself, and on the other hand, it is limited by the performance of parts [36]. Most of the current research is to use UAM additive technology to manufacture parts composed of different materials and to study their forming mechanism [132,133]. The manufacturing of complex structures is generally the production of parts with complex channels. LMD as a kind of near-net-shape technology, the technology has its own unique advantages, although the forming accuracy of this technology is far less than that of PBF technology, but in the face of the production and repair of large parts, this technology can play a huge role [134–136]. LMD technology is the same as SLM technology, which uses laser as the heat source. In recent years, LMD technology has attracted much attention in the industry. L. Arregui et al. [137] studied the geometric limitations of LMD additive manufacturing metal parts in 2018. The results show

---

that good forming parts can be obtained for 60–90° in the case of not adjusting the laser head. S. Singh et al. [138] detected the 1–3 mm cladding layer of pure copper produced by LMD and found that its binding strength could reach 48 MPa, and its corrosion resistance was good. It could be preserved for many years under active corrosion conditions, but the problem of pores still needed to be solved urgently. S. Yadav et al. [139] determined the process window of LMD through the process of PBF, and finally obtained the formed parts with a density of up to 99%, whose tensile properties were higher than those of traditional copper parts after testing.

Pure copper except for good conductive and thermally conductive properties, also have antibacterial and catalytic effects [140,141]. In the study of Y. Wang et al. [142], alternately deposited nickel-copper coatings were produced to provide both excellent wear resistance and antimicrobial properties. This provides new ideas and directions for the application of pure copper, which can be combined with other metals to produce complex medical tools. At the same time, in the study of Y Chong et al. [143], they found that Cu<sub>0</sub> could catalyze the decomposition of azo compounds, and the use of nanoporous structure not only increased the specific surface area, but also avoided the waste of raw materials so that the catalyst could be recycled

## 5. Conclusions

This article reviews three methods of additive manufacturing. The ability to process complex pure copper parts under different methods is compared, and the forming ability under different methods is analyzed. Finally, the mechanical and physical properties of parts produced by SLM, SEBM and BJ additive manufacturing technology are compared. The potential of additive manufacturing has not been fully explored, and the task of researchers is still very heavy. Currently, people are just beginning to understand the process and realize the potential of additive manufacturing. In the future development, better process control is needed to further improve the forming and performance of parts. Different processing methods have different advantages, and the unremitting efforts of researchers will eventually promote the progress of pure copper parts production. Driven by these technologies, it is expected that solutions to the challenge of processing pure copper parts will be found and accelerate the development and progress of various industries.

**Author Contributions:** Conceptualization, P.Z.; methodology, Q.J.; software, D.W.; validation, Z.Y.; formal analysis, H.S.; investigation, H.Y.; resources, P.Z.; data curation, X.Y.; writing—original draft preparation, Q.J.; writing—review and editing, Q.L.; visualization, Y.T.; supervision, Z.Y.; project administration, P.Z.; funding acquisition, P.Z. All authors have read and agreed to the published version of the manuscript.

**Funding:** This research was supported by Foundation of Natural Science Foundation of China (52075317, 51905333), Shanghai Sailing Program (19YF1418100), Shanghai Science and Technology Committee Innovation Grant (19511106400, 19511106402), Shanghai local colleges and universities capacity building special plan project (19030501300).

**Institutional Review Board Statement:** Not applicable.

**Informed Consent Statement:** Not applicable.

**Data Availability Statement:** Not applicable.

**Acknowledgments:** The authors appreciate the facility support by School of Materials Engineering, Shanghai University of Engineering Science, Shanghai.

**Conflicts of Interest:** The authors declare no conflict of interest.

## References

1. Jadhav, S.D.; Dadbakhsh, S.; Vleugels, J.; Hofkens, J.; van Puyvelde, P.; Yang, S.; Kruth, J.P.; Van Humbeeck, J.; Vanmeensel, K. Influence of carbon nanoparticle addition (and impurities) on selective laser melting of pure copper. *Materials* **2019**, *12*, 2469, doi:10.3390/ma12152469.
2. Ikeshoji, T.T.; Nakamura, K.; Yonehara, M.; Imai, K.; Kyogoku, H. Selective Laser Melting of Pure Copper. *Jom* **2018**, *70*, 396–400, doi:10.1007/s11837-017-2695-x.
3. Mao, Z.; Zhang, D.Z.; Wei, P.; Zhang, K. Manufacturing feasibility and forming properties of Cu-4Sn in selective laser melting. *Materials* **2017**, *10*, 333, doi:10.3390/ma10040333.
4. Guschlbauer, R.; Momeni, S.; Osmanlic, F.; Körner, C. Process development of 99.95% pure copper processed via selective electron beam melting and its mechanical and physical properties. *Mater. Charact.* **2018**, *143*, 163–170, doi:10.1016/j.matchar.2018.04.009.
5. Trevisan, F.; Calignano, F.; Lorusso, M.; Lombardi, M.; Manfredi, D.; Fino, P. Selective Laser Melting of Chemical Pure Copper Powders. In Proceedings of the Euro PM2017 Congress & Exhibition, Milan, Italy, 1–5 October 2017.

6. Ledford, C.; Rock, C.; Carriere, P.; Frigola, P.; Gamzina, D.; Horn, T. Characteristics and processing of hydrogen-treated copper powders for EB-PBF additive manufacturing. *Appl. Sci.* **2019**, *9*, 3993, doi:10.3390/app9193993.
7. Jadhav, S.D.; Vleugels, J.; Kruth, J.; Van Humbeeck, J.; Vanmeensel, K. Mechanical and electrical properties of selective laser-melted parts produced from surface-oxidized copper powder. *Mater. Des. Process. Commun.* **2020**, *2*, 1–8, doi:10.1002/mdp2.94.
8. Colopi, M.; Demir, A.G.; Caprio, L.; Previtali, B. Limits and solutions in processing pure Cu via selective laser melting using a high-power single-mode fiber laser. *Int. J. Adv. Manuf. Technol.* **2019**, *104*, 2473–2486, doi:10.1007/s00170-019-04015-3.
9. Yan, X.; Chang, C.; Dong, D.; Gao, S.; Wenyong, M.A.; Liu, M.; Liao, H.; Yin, S. Microstructure and mechanical properties of pure copper manufactured by selective laser melting. *Mater. Sci. Eng. A* **2020**, *789*, 139615, doi:10.1016/j.msea.2020.139615.
10. Lykov, P.A.; Safonov, E.V.; Akhmedianov, A.M. Selective laser melting of copper. *Mater. Sci. Forum* **2016**, *843*, 284–288, doi:10.4028/www.scientific.net/MSF.843.284.
11. Singer, F.; Deisenroth, D.C.; Hymas, D.M.; Ohadi, M.M. Additively manufactured copper components and composite structures for thermal management applications. In Proceedings of the 2017 16th IEEE Intersociety Conference on Thermal and Thermomechanical Phenomena in Electronic Systems (ITherm) IEEE, Orlando, Florida, USA, 30 May–2 June 2017; pp. 174–183.
12. Huang, J.; Yan, X.; Chang, C.; Xie, Y.; Ma, W.; Huang, R.; Zhao, R.; Li, S.; Liu, M.; Liao, H. Pure copper components fabricated by cold spray (CS) and selective laser melting (SLM) technology. *Surf. Coatings Technol.* **2020**, *186*, 125936, doi:10.1016/j.surfcoat.2020.125936.
13. Constantin, L.; Wu, Z.; Li, N.; Fan, L.; Silvain, J.-F.; Lu, Y.F. Laser 3D printing of Complex Copper Structures. *Addit. Manuf.* **2020**, *35*, 101268, doi:10.1016/j.addma.2020.101268.
14. Wang, X.; Liu, J.; Wang, Y.; Fu, Y. Fabrication of friction-reducing texture surface by selective laser melting of ink-printed (SLM-IP) copper (Cu) nanoparticles (NPs). *Appl. Surf. Sci.* **2017**, *396*, 659–664, doi:10.1016/j.apsusc.2016.11.003.
15. Pathak, S.; Saha, G.C. Development of sustainable cold spray coatings and 3D additive manufacturing components for repair/manufacturing applications: A critical review. *Coatings* **2017**, *7*, 122, doi:10.3390/coatings7080122.
16. Gradl, P.R.; Protz, C.S.; Ellis, D.L.; Greene, S.E. Progress in additively manufactured copper-alloy GRCOP-84, GRCOP-42, and bimetallic combustion chambers for liquid rocket engines. *Proc. Int. Astronaut. Congr. IAC* **2019**, *2019*, 21–25.
17. Singh, R.; Gupta, A.; Tripathi, O.; Srivastava, S.; Singh, B.; Awasthi, A.; Rajput, S.K.; Sonia, P.; Singhal, P.; Saxena, K.K. Powder bed fusion process in additive manufacturing: An overview. *Mater. Today Proc.* **2020**, *26*, 3058–3070, doi:10.1016/j.matpr.2020.02.635.
18. Duta, L.; Neamtu, J.; Melinte, R.P.; Zureigat, O.A.; Popescu-Pelin, G.; Chioibasu, D.; Oktar, F.N.; Popescu, A.C. In vivo assessment of bone enhancement in the case of 3d-printed implants functionalized with lithium-doped biological-derived hydroxyapatite coatings: A preliminary study on rabbits. *Coatings* **2020**, *10*, 992, doi:10.3390/coatings10100992.
19. Tran, T.Q.; Chinnappan, A.; Lee, J.K.Y.; Loc, N.H.; Tran, L.T.; Wang, G.; Kumar, V.V.; Jayathilaka, W.A.D.M.; Ji, D.; Doddamani, M.; et al. 3D printing of highly pure copper. *Metals* **2019**, *9*, 756, doi:10.3390/met9070756.
20. Rahmani, R.; Antonov, M.; Prashanth, K.G. The impact resistance of highly densified metal alloys manufactured from gas-atomized pre-alloyed powders. *Coatings* **2021**, *11*, 216, doi:10.3390/coatings11020216.
21. Pobel, C.R.; Lodes, M.A.; Körner, C. Selective Electron Beam Melting of Oxide Dispersion Strengthened Copper. *Adv. Eng. Mater.* **2018**, *20*, 1–7, doi:10.1002/adem.201800068.
22. Tümer, E.H.; Erbil, H.Y. Extrusion-Based 3D Printing Applications of PLA Composites: A Review. *Coatings* **2021**, *11*, 390, doi:10.3390/coatings11040390.
23. Brandl, E.; Michailov, V.; Viehweger, B.; Leyens, C. Deposition of Ti-6Al-4V using laser and wire, part I: Microstructural properties of single beads. *Surf. Coatings Technol.* **2011**, *206*, 1120–1129, doi:10.1016/j.surfcoat.2011.07.095.
24. Dssolfdwlrqv, W.S.; Sdshu, Q.W.; Uhsruw, Z.H.; Wkhq, W.L.V.; Wkdw, V.; Pdqidfwxuhg, D.; Wr, O.; Dqg, G.; Ilw, P.; Ixqfwlrq, D.Q.G.; et al. Selective laser sintering of composite copper-tin powders. *Mater. Today Commun.* **2020**, *24*, 101195, doi:10.1016/j.addma.2020.101268.
25. Körner, C. Additive manufacturing of metallic components by selective electron beam melting—A review. *Int. Mater. Rev.* **2016**, *61*, 361–377, doi:10.1080/09506608.2016.1176289.
26. Markl, M.; Lodes, M.; Franke, M.; Körner, C. Additive manufacturing using selective electron beam melting. *Weld. Cut.* **2017**, *16*, 177–184.
27. Silbernagel, C.; Gargalis, L.; Ashcroft, I.; Hague, R.; Galea, M.; Dickens, P. Electrical resistivity of pure copper processed by medium-powered laser powder bed fusion additive manufacturing for use in electromagnetic applications. *Addit. Manuf.* **2019**, *29*, 100831, doi:10.1016/j.addma.2019.100831.
28. Guschlbauer, R.; Burkhardt, A.K.; Fu, Z.; Körner, C. Effect of the oxygen content of pure copper powder on selective electron beam melting. *Mater. Sci. Eng. A* **2020**, *779*, 139106, doi:10.1016/j.msea.2020.139106.
29. Bai, Y.; Williams, C.B. An exploration of binder jetting of copper. *Rapid Prototyp. J.* **2015**, *21*, 177–185, doi:10.1108/RPJ-12-2014-0180.

- 
30. Zhong, H.Z.; Li, C.G.; Zhang, X.Y.; Gu, J.F. The graded microstructures evolving with thermal cycles in pure copper processed by laser metal deposition. *Mater. Lett.* **2018**, *230*, 215–218, doi:10.1016/j.matlet.2018.07.105.
  31. Sriraman, M.R.; Gonser, M.; Fujii, H.T.; Babu, S.S.; Bloss, M. Thermal transients during processing of materials by very high power ultrasonic additive manufacturing. *J. Mater. Process. Technol.* **2011**, *211*, 1650–1657, doi:10.1016/j.jmatprotec.2011.05.003.
  32. Ashkenazi, D.; Inberg, A.; Shacham-Diamand, Y.; Stern, A. Gold, Silver, and Electrum Electroless Plating on Additively Manufactured Laser Powder-Bed Fusion AlSi10Mg Parts: A Review. *Coatings* **2021**, *11*, 422, doi:10.3390/coatings11040422.
  33. Lehnert, R.; Wagner, R.; Burkhardt, C.; Clausnitzer, P.; Weidner, A.; Wendler, M.; Volkova, O.; Biermann, H. Microstructural and mechanical characterization of high-alloy quenching and partitioning TRIP steel manufactured by electron beam melting. *Mater. Sci. Eng. A* **2020**, *794*, 139684, doi:10.1016/j.msea.2020.139684.
  34. Heßelmann, C.; Wolf, T.; Galgon, F.; Körner, C.; Albert, J.; Wasserscheid, P. Additively manufactured RANEY®-type copper catalyst for methanol synthesis. *Catal. Sci. Technol.* **2020**, *10*, 164–168, doi:10.1039/c9cy01657k.
  35. Tan, H.; Guo, M.; Clare, A.T.; Lin, X.; Chen, J.; Huang, W. Microstructure and properties of Ti-6Al-4V fabricated by low-power pulsed laser directed energy deposition. *J. Mater. Sci. Technol.* **2019**, *35*, 2027–2037, doi:10.1016/j.jmst.2019.05.008.
  36. Sridharan, N.; Wolcott, P.; Dapino, M.; Babu, S.S. Microstructure and texture evolution in aluminum and commercially pure titanium dissimilar welds fabricated using ultrasonic additive manufacturing. *Scr. Mater.* **2016**, *117*, 1–5, doi:10.1016/j.scriptamat.2016.02.013.
  37. Imai, K.; Ikeshoji, T.; Sugitani, Y.; Kyogoku, H. Densification of pure copper by selective laser melting process. *Mech. Eng. J.* **2020**, *7*, 272, doi:10.1299/mej.19-00272.
  38. Raab, S.J.; Guschlbauer, R.; Lodes, M.A.; Körner, C. Thermal and Electrical Conductivity of 99.9% Pure Copper Processed via Selective Electron Beam Melting. *Adv. Eng. Mater.* **2016**, *18*, 1661–1666, doi:10.1002/adem.201600078.
  39. Jadhav, S.D.; Dadbakhsh, S.; Goossens, L.; Kruth, J.P.; Van Humbeeck, J.; Vanmeensel, K. Influence of selective laser melting process parameters on texture evolution in pure copper. *J. Mater. Process. Technol.* **2019**, *270*, 47–58, doi:10.1016/j.jmatprotec.2019.02.022.
  40. Guan, J.; Zhang, X.; Jiang, Y.; Yan, Y. Insights into fabrication mechanism of pure copper thin wall components by selective infrared laser melting. *Rapid Prototyp. J.* **2019**, *25*, 1388–1397, doi:10.1108/RPJ-06-2018-0143.
  41. Yan, X.; Chang, C.; Dong, D.; Gao, S.; Wenyong, M.A.; Liu, M.; Liao, H.; Yin, S. Microstructure and mechanical properties of pure copper manufactured by selective laser melting. *Mater. Sci. Eng. A* **2020**, *789*, 139615, doi:10.1016/j.msea.2020.139615.
  42. Santo, L.; Quadrini, F.; Bellisario, D.; Tedde, G.M.; Zarccone, M.; Di Domenico, G.; D'Angelo, P.; Corona, D. Local density measurement of additive manufactured copper parts by instrumented indentation. *AIP Conf. Proc.* **2018**, *1960*, 100014, doi:10.1063/1.5034954.
  43. Colopi, M.; Caprio, L.; Demir, A.G.; Previtali, B. Selective laser melting of pure Cu with a 1 kW single mode fiber laser. *Procedia CIRP* **2018**, *74*, 59–63, doi:10.1016/j.procir.2018.08.030.
  44. Lykov, P.; Baytmerov, R.; Vaulin, S.; Safonov, E.; Zhrebtsov, D. Selective Laser Melting of Copper by 200 W CO<sub>2</sub> Laser. *SAE Tech. Pap.* **2016**, *1*, 2016–2019, doi:10.4271/2016-01-0333.
  45. Zhang, D.Q.; Liu, Z.H.; Chua, C.K. Investigation on Forming Process of Copper Alloys via Selective Laser Melting. In High Value Manufacturing: Advanced Research in Virtual and Rapid Prototyping. In Proceedings of the 6th International Conference on Advanced Research in Virtual and Rapid Prototyping, Leiria, Portugal, 1–5 October 2013; Taylor&Francis Group: London, UK, 2014; pp. 285–289, doi:10.1201/b15961-53.
  46. Guschlbauer, R.; Momeni, S.; Osmanlic, F.; Körner, C. Process development of 99.95% pure copper processed via selective electron beam melting and its mechanical and physical properties. *Mater. Charact.* **2018**, *143*, 163–170, doi:10.1016/j.matchar.2018.04.009.
  47. Lodes, M.A.; Guschlbauer, R.; Körner, C. Process development for the manufacturing of 99.94% pure copper via selective electron beam melting. *Mater. Lett.* **2015**, *143*, 298–301, doi:10.1016/j.matlet.2014.12.105.
  48. Ramirez, D.A.; Murr, L.E.; Martinez, E.; Hernandez, D.H.; Martinez, J.L.; MacHado, B.I.; Medina, F.; Frigola, P.; Wicker, R.B. Novel precipitate-microstructural architecture developed in the fabrication of solid copper components by additive manufacturing using electron beam melting. *Acta Mater.* **2011**, *59*, 4088–4099, doi:10.1016/j.actamat.2011.03.033.
  49. Frigola, P.; Harrysson, O.A.; Horn, T.J.; West, H.A.; Aman, R.L.; Rigsbee, J.M.; Ramirez, D.A.; Murr, L.E.; Medina, F.; Wicker, R.B.; et al. Fabricating Copper Components with Electron Beam Melting. *Adv. Mater. Process.* **2014**, *172*, 20–24.
  50. Yegyan-Kumar, A.; Wang, J.; Bai, Y.; Huxtable, S.T.; Williams, C.B. Impacts of process-induced porosity on material properties of copper made by binder jetting additive manufacturing. *Mater. Des.* **2019**, *182*, 108001, doi:10.1016/j.matdes.2019.108001.
  51. Singh, G.; Pandey, P.M. Experimental investigations into mechanical and thermal properties of rapid manufactured copper parts. *Proc. Inst. Mech. Eng. Part C J. Mech. Eng. Sci.* **2020**, *234*, 82–95, doi:10.1177/0954406219875483.
  52. Oliveira, J.P.; La Londe, A.D.; Ma, J. Processing parameters in laser powder bed fusion metal additive manufacturing. *Mater. Des.* **2020**, *193*, 1–12, doi:10.1016/j.matdes.2020.108762.

- 
53. Fotovvati, B.; Balasubramanian, M.; Asadi, E. Modeling and Optimization Approaches of Laser-Based Powder-Bed Fusion Process for Ti-6Al-4V Alloy. *Coatings* **2020**, *10*, 1104, doi:10.3390/coatings10111104.
  54. Siddaiah, A.; Kasar, A.; Kumar, P.; Akram, J.; Misra, M.; Menezes, P.L. Tribocorrosion behavior of inconel 718 fabricated by laser powder bed fusion-based additive manufacturing. *Coatings* **2021**, *11*, 195, doi:10.3390/coatings11020195.
  55. Luo, Z.; Zhao, Y. A survey of finite element analysis of temperature and thermal stress fields in powder bed fusion Additive Manufacturing. *Addit. Manuf.* **2018**, *21*, 318–332, doi:10.1016/j.addma.2018.03.022.
  56. Mahmood, M.A.; Bănică, A.; Ristoscu, C.; Becherescu, N.; Mihăilescu, I.N. Laser coatings via state-of-the-art additive manufacturing: A review. *Coatings* **2021**, *11*, 296, doi:10.3390/coatings11030296.
  57. Bartlett, J.L.; Li, X. An overview of residual stresses in metal powder bed fusion. *Addit. Manuf.* **2019**, *27*, 131–149, doi:10.1016/j.addma.2019.02.020.
  58. Afkhami, S.; Piili, H.; Salminen, A.; Björk, T. Effective parameters on the fatigue life of metals processed by powder bed fusion technique: A short review. *Procedia Manuf.* **2019**, *36*, 3–10, doi:10.1016/j.promfg.2019.08.002.
  59. Kalms, M.; Narita, R.; Thomy, C.; Vollertsen, F.; Bergmann, R.B. New approach to evaluate 3D laser printed parts in powder bed fusion-based additive manufacturing in-line within closed space. *Addit. Manuf.* **2019**, *26*, 161–165, doi:10.1016/j.addma.2019.01.011.
  60. Liu, Y.; Blunt, L.; Zhang, Z.; Rahman, H.A.; Gao, F.; Jiang, X. In-situ areal inspection of powder bed for electron beam fusion system based on fringe projection profilometry. *Addit. Manuf.* **2020**, *31*, 100940, doi:10.1016/j.addma.2019.100940.
  61. Chen, Q.; Guillemot, G.; Gandin, C.A.; Bellet, M. Three-dimensional finite element thermomechanical modeling of additive manufacturing by selective laser melting for ceramic materials. *Addit. Manuf.* **2017**, *16*, 124–137, doi:10.1016/j.addma.2017.02.005.
  62. Sing, S.L.; Huang, S.; Yeong, W.Y. Effect of solution heat treatment on microstructure and mechanical properties of laser powder bed fusion produced cobalt-28chromium-6molybdenum. *Mater. Sci. Eng. A* **2020**, *769*, 138511, doi:10.1016/j.msea.2019.138511.
  63. Gu, D.; Shen, Y.; Fang, S.; Xiao, J. Metallurgical mechanisms in direct laser sintering of Cu-CuSn-CuP mixed powder. *J. Alloys Compd.* **2007**, *438*, 184–189, doi:10.1016/j.jallcom.2006.08.040.
  64. Tang, Y.; Loh, H.T.; Wong, Y.S.; Fuh, J.Y.H.; Lu, L.; Wang, X. Direct laser sintering of a copper-based alloy for creating three-dimensional metal parts. *J. Mater. Process. Technol.* **2003**, *140*, 368–372, doi:10.1016/s0924-0136(03)00766-0.
  65. Khan, K.; Mohr, G.; Hilgenberg, K.; De, A. Probing a novel heat source model and adaptive remeshing technique to simulate laser powder bed fusion with experimental validation. *Comput. Mater. Sci.* **2020**, *181*, 109752, doi:10.1016/j.commatsci.2020.109752.
  66. Robinson, J.; Stanford, M.; Arjunan, A. Stable formation of powder bed laser fused 99.9% silver. *Mater. Today Commun.* **2020**, *24*, 101195, doi:10.1016/j.mtcomm.2020.101195.
  67. Sauerbier, P.; Anderson, J.; Gardner, D.J. Surface preparation and treatment for large-scale 3D-printed composite tooling coating adhesion. *Coatings* **2018**, *8*, 457, doi:10.3390/COATINGS8120457.
  68. Sendino, S.; Gardon, M.; Lartategui, F.; Martinez, S.; Lamikiz, A. The effect of the laser incidence angle in the surface of l-pbf processed parts. *Coatings* **2020**, *10*, 1024, doi:10.3390/coatings10111024.
  69. Wang, X.; Liu, J.; Yang, L.; He, Y.; Wang, Y. Nano-sized amorphous carbon covered surface formed by selective laser melting of ink-printed (SLM-IP) copper (Cu) nanoparticles (NPs). *Appl. Surf. Sci.* **2018**, *448*, 133–137, doi:10.1016/j.apsusc.2018.04.109.
  70. Wang, X.; Liu, J.; He, Y.; Wang, Y. Selective laser melting of ink-printed (SLM-IP) copper (Cu) nanoparticles (NPs) for facile controllable fabrication of super-hydrophobic surface. *Surf. Coatings Technol.* **2018**, *347*, 84–91, doi:10.1016/j.surfcoat.2018.04.080.
  71. Siva Prasad, H.; Brueckner, F.; Volpp, J.; Kaplan, A.F.H. Laser metal deposition of copper on diverse metals using green laser sources. *Int. J. Adv. Manuf. Technol.* **2020**, *107*, 1559–1568, doi:10.1007/s00170-020-05117-z.
  72. Wang, H.; Kawahito, Y.; Yoshida, R.; Nakashima, Y.; Shiokawa, K. Development of a high-power blue laser (445 nm) for material processing. *Opt. Lett.* **2017**, *42*, 2251, doi:10.1364/ol.42.002251.
  73. Sinico, M.; Cogo, G.; Benettoni, M.; Calliari, I.; Pepato, A. Influence of powder particle size distribution on the printability of pure copper for selective laser melting. In Proceedings of the 30th Annual International Solid Freeform Fabrication Symposium—An Additive Manufacturing Conference, Austin, TX, USA, 12–14 August 2019; pp. 657–667.
  74. Wolf, T.; Fu, Z.; Körner, C. Selective electron beam melting of an aluminum bronze: Microstructure and mechanical properties. *Mater. Lett.* **2019**, *238*, 241–244, doi:10.1016/j.matlet.2018.12.015.
  75. Schaub, A.; Juechter, V.; Singer, R.F.; Merklein, M. Characterization of hybrid components consisting of SEBM additive structures and sheet metal of alloy Ti-6Al-4V. *Key Eng. Mater.* **2014**, *611–612*, 609–614, doi:10.4028/www.scientific.net/KEM.611-612.609.
  76. Schwerdtfeger, J.; Schury, F.; Stingl, M.; Wein, F.; Singer, R.F.; Körner, C. Mechanical characterisation of a periodic auxetic structure produced by SEBM. *Phys. Status Solidi Basic Res.* **2012**, *249*, 1347–1352, doi:10.1002/pssb.201084211.
  77. Tang, H.P.; Wang, J.; Song, C.N.; Liu, N.; Jia, L.; Elambasseril, J.; Qian, M. Microstructure, Mechanical Properties, and Flatness of SEBM Ti-6Al-4V Sheet in As-Built and Hot Isostatically Pressed Conditions. *Jom* **2017**, *69*, 466–471, doi:10.1007/s11837-016-2253-y.

- 
78. Yang, G.; Jia, W.; Zhao, P.; Jia, L.; Liu, N.; Wang, J.; Tang, H. Microstructures of as-fabricated and post heat treated Ti-47Al-2Nb-2Cr alloy produced by selective electron beam melting (SEBM). *Rare Met. Mater. Eng.* **2016**, *45*, 1683–1686, doi:10.1016/s1875-5372(16)30140-0.
  79. Wang, J.; Tang, H. Review on metals additively manufactured by SEBM. *Mater. Technol.* **2016**, *31*, 86–89, doi:10.1179/1753555715Y.0000000081.
  80. Zhang, X.Z.; Tang, H.P.; Leary, M.; Song, T.; Jia, L.; Qian, M. Toward Manufacturing Quality Ti-6Al-4V Lattice Struts by Selective Electron Beam Melting (SEBM) for Lattice Design. *Jom* **2018**, *70*, 1870–1876, doi:10.1007/s11837-018-3030-x.
  81. Sun, Y.Y.; Gulizia, S.; Fraser, D.; Oh, C.H.; Lu, S.L.; Qian, M. Layer Additive Production or Manufacturing of Thick Sections of Ti-6Al-4V by Selective Electron Beam Melting (SEBM). *Jom* **2017**, *69*, 1836–1843, doi:10.1007/s11837-017-2462-z.
  82. Zhao, Y.; Koizumi, Y.; Aoyagi, K.; Wei, D.; Yamanaka, K.; Chiba, A. Molten pool behavior and effect of fluid flow on solidification conditions in selective electron beam melting (SEBM) of a biomedical Co-Cr-Mo alloy. *Addit. Manuf.* **2019**, *26*, 202–214, doi:10.1016/j.addma.2018.12.002.
  83. Sing, S.L.; An, J.; Yeong, W.Y.; Wiria, F.E. Laser and electron-beam powder-bed additive manufacturing of metallic implants: A review on processes, materials and designs. *J. Orthop. Res.* **2016**, *34*, 369–385, doi:10.1002/jor.23075.
  84. Yang, G.; Yang, P.; Yang, K.; Liu, N.; Jia, L.; Wang, J.; Tang, H. Effect of processing parameters on the density, microstructure and strength of pure tungsten fabricated by selective electron beam melting. *Int. J. Refract. Met. Hard Mater.* **2019**, *84*, 105040, doi:10.1016/j.ijrmhm.2019.105040.
  85. Warmuth, F.; Osmanlic, F.; Adler, L.; Lodes, M.A.; Körner, C. Fabrication and characterisation of a fully auxetic 3D lattice structure via selective electron beam melting. *Smart Mater. Struct.* **2017**, *26*, 025013, doi:10.1088/1361-665X/26/2/025013.
  86. Juechter, V.; Körner, C. Creep properties of Ti-48Al-2Cr-2Nb produced by selective electron beam melting. *Key Eng. Mater.* **2016**, *704*, 190–196, doi:10.4028/www.scientific.net/KEM.704.190.
  87. Ledford, C.; Rock, C.; Tung, M.; Wang, H.; Schroth, J.; Horn, T. Evaluation of Electron Beam Powder Bed Fusion Additive Manufacturing of High Purity Copper for Overhang Structures Using In-Situ Real Time Backscatter Electron Monitoring. *Procedia Manuf.* **2020**, *48*, 828–838, doi:10.1016/j.promfg.2020.05.120.
  88. Miyanaji, H.; Orth, M.; Akbar, J.M.; Yang, L. Process development for green part printing using binder jetting additive manufacturing. *Front. Mech. Eng.* **2018**, *13*, 504–512, doi:10.1007/s11465-018-0508-8.
  89. Wheat, E.; Vlasea, M.; Hinebaugh, J.; Metcalfe, C. Sinter structure analysis of titanium structures fabricated via binder jetting additive manufacturing. *Mater. Des.* **2018**, *156*, 167–183, doi:10.1016/j.matdes.2018.06.038.
  90. Wang, Y.; Zhao, Y.F. Investigation of Sintering Shrinkage in Binder Jetting Additive Manufacturing Process. *Procedia Manuf.* **2017**, *10*, 779–790, doi:10.1016/j.promfg.2017.07.077.
  91. Gonzalez, J.A.; Mireles, J.; Lin, Y.; Wicker, R.B. Characterization of ceramic components fabricated using binder jetting additive manufacturing technology. *Ceram. Int.* **2016**, *42*, 10559–10564, doi:10.1016/j.ceramint.2016.03.079.
  92. Meteyer, S.; Xu, X.; Perry, N.; Zhao, Y.F. Energy and material flow analysis of binder-jetting additive manufacturing processes. *Procedia CIRP* **2014**, *15*, 19–25, doi:10.1016/j.procir.2014.06.030.
  93. Gaytan, S.M.; Cadena, M.A.; Karim, H.; Delfin, D.; Lin, Y.; Espalin, D.; MacDonald, E.; Wicker, R.B. Fabrication of barium titanate by binder jetting additive manufacturing technology. *Ceram. Int.* **2015**, *41*, 6610–6619, doi:10.1016/j.ceramint.2015.01.108.
  94. Bai, Y.; Wagner, G.; Williams, C.B. Effect of bimodal powder mixture on powder packing density and sintered density in binder jetting of metals. *Annu. Int. Solid Free. Fabr. Symp.* **2015**, *62*, 758–771.
  95. Gokuldoss, P.K.; Kolla, S.; Eckert, J. Additive manufacturing processes: Selective laser melting, electron beam melting and binder jetting-selection guidelines. *Materials* **2017**, *10*, 672, doi:10.3390/ma10060672.
  96. Bai, Y.; Williams, C.B. An exploration of binder jetting of copper. *Rapid Prototyp. J.* **2015**, *21*, 177–185, doi:10.1108/RPJ-12-2014-0180.
  97. Mostafaei, A.; Stevens, E.L.; Hughes, E.T.; Biery, S.D.; Hilla, C.; Chmielus, M. Powder bed binder jet printed alloy 625: Densification, microstructure and mechanical properties. *Mater. Des.* **2016**, *108*, 126–135, doi:10.1016/j.matdes.2016.06.067.
  98. Singh, S.; Ramakrishna, S.; Singh, R. Material issues in additive manufacturing: A review. *J. Manuf. Process.* **2017**, *25*, 185–200, doi:10.1016/j.jmapro.2016.11.006.
  99. Horn, T.J.; Harrysson, O.L.A. Overview of Current Additive Manufacturing Technologies and Selected Applications. *Sci. Prog.* **2012**, *95*, 255–282, doi:10.3184/003685012X13420984463047.
  100. Ngo, T.D.; Kashani, A.; Imbalzano, G.; Nguyen, K.T.Q.; Hui, D. Additive manufacturing (3D printing): A review of materials, methods, applications and challenges. *Compos. Part B Eng.* **2018**, *143*, 172–196, doi:10.1016/j.compositesb.2018.02.012.
  101. Heider, A.; Stritt, P.; Hess, A.; Weber, R.; Graf, T. Process stabilization at welding copper by laser power modulation. *Phys. Procedia* **2011**, *12*, 81–87, doi:10.1016/j.phpro.2011.03.011.
  102. Behroozfar, A.; Daryadel, S.; Morsali, S.R.; Moreno, S.; Baniasadi, M.; Bernal, R.A.; Minary-Jolandan, M. Microscale 3D Printing of Nanotwinned Copper. *Adv. Mater.* **2018**, *30*, 1–6, doi:10.1002/adma.201705107.

- 
103. Gu, D.; Shen, Y. Balling phenomena during direct laser sintering of multi-component Cu-based metal powder. *J. Alloys Compd.* **2007**, *432*, 163–166, doi:10.1016/j.jallcom.2006.06.011.
  104. Zhu, H.H.; Lu, L.; Fuh, J.Y.H. Development and characterisation of direct laser sintering Cu-based metal powder. *J. Mater. Process. Technol.* **2003**, *140*, 314–317, doi:10.1016/S0924-0136(03)00755-6.
  105. Kaden, L.; Matthäus, G.; Ullsperger, T.; Engelhardt, H.; Rettenmayr, M.; Tünnermann, A.; Nolte, S. Selective laser melting of copper using ultrashort laser pulses. *Appl. Phys. A Mater. Sci. Process.* **2017**, *123*, 1–6, doi:10.1007/s00339-017-1189-6.
  106. Murr, L.E.; Gaytan, S.M.; Ramirez, D.A.; Martinez, E.; Hernandez, J.; Amato, K.N.; Shindo, P.W.; Medina, F.R.; Wicker, R.B. Metal Fabrication by Additive Manufacturing Using Laser and Electron Beam Melting Technologies. *J. Mater. Sci. Technol.* **2012**, *28*, 1–14, doi:10.1016/S1005-0302(12)60016-4.
  107. Qi, Z.; Cong, B.; Qi, B.; Sun, H.; Zhao, G.; Ding, J. Microstructure and mechanical properties of double-wire + arc additively manufactured Al-Cu-Mg alloys. *J. Mater. Process. Technol.* **2018**, *255*, 347–353, doi:10.1016/j.jmatprotec.2017.12.019.
  108. Ramirez, D.A.; Murr, L.E.; Li, S.J.; Tian, Y.X.; Martinez, E.; Martinez, J.L.; Machado, B.I.; Gaytan, S.M.; Medina, F.; Wicker, R.B. Open-cellular copper structures fabricated by additive manufacturing using electron beam melting. *Mater. Sci. Eng. A* **2011**, *528*, 5379–5386, doi:10.1016/j.msea.2011.03.053.
  109. Profile, S.E.E. Pure copper development at industrial scale by electron beam tecnología de fabricación aditiva electron beam melting ( ebm ) pure copper development at industrial scale by. 2019.
  110. Kumar, A.; Bai, Y.; Eklund, A.; Williams, C.B. Effects of Hot Isostatic Pressing on Copper Parts Fabricated via Binder Jetting. *Procedia Manuf.* **2017**, *10*, 935–944, doi:10.1016/j.promfg.2017.07.084.
  111. Miyanaji, H.; Ma, D.; Atwater, M.A.; Darling, K.A.; Hammond, V.H.; Williams, C.B. Binder jetting additive manufacturing of copper foam structures. *Addit. Manuf.* **2020**, *32*, 100960, doi:10.1016/j.addma.2019.100960.
  112. Gibson, B.T.; Lowden, R.A. *Process Development for Selective Laser Melting of Molybdenum*; Oak Ridge National Lab.(ORNL): Oak Ridge, TN, USA, 2018; doi:10.2172/1484987.
  113. Syed-Khaja, A.; Schwarz, D.; Franke, J. Advanced substrate and packaging concepts for compact system integration with additive manufacturing technologies for high temperature applications. *IEEE CPMT Symp. Japan* **2015**, *2015*, 156–159, doi:10.1109/ICSJ.2015.7357402.
  114. Sciammarella, F.; Gonser, M.J.; Styracula, M. Laser Additive Manufacturing of Pure Copper. *Rapid* **2013**.
  115. Yin, J.; Yang, L.L.; Yang, X.; Zhu, H.; Wang, D.; Ke, L.; Wang, Z.; Wang, G.; Zeng, X. High-power laser-matter interaction during laser powder bed fusion. *Addit. Manuf.* **2019**, *29*, 100778, doi:10.1016/j.addma.2019.100778.
  116. Momeni, S.; Guschlbauer, R.; Osmanlic, F.; Körner, C. Selective electron beam melting of a copper-chrome powder mixture. *Mater. Lett.* **2018**, *223*, 250–252, doi:10.1016/j.matlet.2018.03.194.
  117. Bai, Y.; Wagner, G.; Williams, C.B. Effect of particle size distribution on powder packing and sintering in binder jetting additive manufacturing of metals. *J. Manuf. Sci. Eng. Trans. ASME* **2017**, *139*, 1–15, doi:10.1115/1.4036640.
  118. Rishmawi, I.; Salarian, M.; Vlasea, M. Tailoring green and sintered density of pure iron parts using binder jetting additive manufacturing. *Addit. Manuf.* **2018**, *24*, 508–520, doi:10.1016/j.addma.2018.10.015.
  119. Bai, Y.; Williams, C.B. The effect of inkjetted nanoparticles on metal part properties in binder jetting additive manufacturing. *Nanotechnology* **2018**, *29*, 395706, doi:10.1088/1361-6528/aad0bb.
  120. Abdi, F.; Yavari, P.; Harik, V.; Godines, C. Material allowable generation and AM process parameters effect on porosity. *Coatings* **2020**, *10*, 625, doi:10.3390/coatings10070625.
  121. Karakurt, I.; Ho, K.Y.; Ledford, C.; Gamzina, D.; Horn, T.; Luhmann, N.C.; Lin, L. Development of a magnetically driven abrasive polishing process for additively manufactured copper structures. *Procedia Manuf.* **2018**, *26*, 798–805, doi:10.1016/j.promfg.2018.07.097.
  122. El-Wardany, T.I.; She, Y.; Jagdale, V.N.; Garofano, J.K.; Liou, J.J.; Schmidt, W.R. Challenges in Three-Dimensional Printing of High-Conductivity Copper. *J. Electron. Packag. Trans. ASME* **2018**, *140*, 1–12, doi:10.1115/1.4039974.
  123. Monaghan, T.; Capel, A.J.; Christie, S.D.; Harris, R.A.; Friel, R.J. Solid-state additive manufacturing for metallized optical fiber integration. *Compos. Part A Appl. Sci. Manuf.* **2015**, *76*, 181–193, doi:10.1016/j.compositesa.2015.05.032.
  124. Jucan, O.D.; Gădălean, R.V.; Chicinaș, H.F.; Hering, M.; Bâlc, N.; Popa, C.O. Study on the indirect selective laser sintering (SLS) of WC-Co/PA12 powders for the manufacturing of cemented carbide parts. *Int. J. Refract. Met. Hard Mater.* **2021**, *96*, 2–10, doi:10.1016/j.ijrmhm.2021.105498.
  125. Hussain, G.; Khan, W.A.; Ashraf, H.A.; Ahmad, H.; Ahmed, H.; Imran, A.; Ahmad, I.; Rehman, K.; Abbas, G. Design and development of a lightweight SLS 3D printer with a controlled heating mechanism: Part A. *Int. J. Light. Mater. Manuf.* **2019**, *2*, 373–378, doi:10.1016/j.ijlmm.2019.01.005.
  126. Amorim, F.L.; Lohregel, A.; Müller, N.; Schäfer, G.; Czelusniak, T. Performance of sinking EDM electrodes made by selective laser sintering technique. *Int. J. Adv. Manuf. Technol.* **2013**, *65*, 1423–1428, doi:10.1007/s00170-012-4267-0.
  127. Kuo, C.H.; Sridharan, N.; Han, T.; Dapino, M.J.; Babu, S.S. Ultrasonic additive manufacturing of 4130 steel using Ni interlayers\*. *Sci. Technol. Weld. Join.* **2019**, *24*, 382–390, doi:10.1080/13621718.2019.1607486.
  128. Gibert, J.M.; Fadel, G.; Daqaq, M.F. On the stick-slip dynamics in ultrasonic additive manufacturing. *J. Sound Vib.* **2013**, *332*, 4680–4695, doi:10.1016/j.jsv.2013.04.007.
  129. Martin, J.D. Imece2017-71685 Exploring Additive Manufacturing Processes for Direct 3D. **2017**, 3–9.

- 
130. Wang, Y.; Yang, Q.; Liu, X.; Liu, Y.; Liu, B.; Misra, R.D.K.; Xu, H.; Bai, P. Microstructure and mechanical properties of amorphous strip/aluminum laminated composites fabricated by ultrasonic additive consolidation. *Mater. Sci. Eng. A* **2019**, *749*, 74–78, doi:10.1016/j.msea.2019.01.039.
  131. Sojiphan, K. Effects of Very High Power Ultrasonic Additive Manufacturing Process Parameters on Hardness, Microstructure, and Texture of Aluminum 3003-H18 Alloy. Ph.D. Thesis, The Ohio State University, Columbus, OH, USA, 2015.
  132. Sriraman, M.R.; Babu, S.S.; Short, M. Bonding characteristics during very high power ultrasonic additive manufacturing of copper. *Scr. Mater.* **2010**, *62*, 560–563, doi:10.1016/j.scriptamat.2009.12.040.
  133. Ward, A.A.; Cordero, Z.C. Junction growth and interdiffusion during ultrasonic additive manufacturing of multi-material laminates. *Scr. Mater.* **2020**, *177*, 101–105, doi:10.1016/j.scriptamat.2019.10.004.
  134. Azarniya, A.; Colera, X.G.; Mirzaali, M.J.; Sovizi, S.; Bartolomeu, F.; St Weglowski, M.K.; Wits, W.W.; Yap, C.Y.; Ahn, J.; Miranda, G.; et al. Additive manufacturing of Ti–6Al–4V parts through laser metal deposition (LMD): Process, microstructure, and mechanical properties. *J. Alloys Compd.* **2019**, *804*, 163–191, doi:10.1016/j.jallcom.2019.04.255.
  135. Cai, Y.; Zhu, L.; Cui, Y.; Han, J. Manufacturing of FeCoCrNi + FeCoCrNiAl laminated high-entropy alloy by laser melting deposition (LMD). *Mater. Lett.* **2021**, *289*, 129445, doi:10.1016/j.matlet.2021.129445.
  136. Kittel, J.; Gasser, A.; Wissenbach, K.; Zhong, C.; Schleifenbaum, J.H.; Palm, F. Case study on AM of an IN718 aircraft component using the LMD process. *Procedia CIRP* **2020**, *94*, 324–329, doi:10.1016/j.procir.2020.09.061.
  137. Arregui, L.; Garmendia, I.; Pujana, J.; Soriano, C. Study of the Geometrical Limitations Associated to the Metallic Part Manufacturing by the LMD Process. *Procedia CIRP* **2018**, *68*, 363–368, doi:10.1016/j.procir.2017.12.096.
  138. Singh, S.; Kumar, M.; Sodhi, G.P.S.; Buddu, R.K.; Singh, H. Development of thick copper claddings on SS316L steel for In-vessel components of fusion reactors and copper-cast iron canisters. *Fusion Eng. Des.* **2018**, *128*, 126–137, doi:10.1016/j.fusengdes.2018.01.076.
  139. Yadav, S.; Paul, C.P.; Jinoop, A.N.; Rai, A.K.; Bindra, K.S. Laser Directed Energy Deposition based Additive Manufacturing of Copper: Process Development and Material Characterizations. *J. Manuf. Process.* **2020**, *58*, 984–997, doi:10.1016/j.jmapro.2020.09.008.
  140. Rivera, L.R.; Cochis, A.; Biser, S.; Canciani, E.; Ferraris, S.; Rimondini, L.; Boccaccini, A.R. Antibacterial, pro-angiogenic and pro-osteointegrative zein-bioactive glass/copper based coatings for implantable stainless steel aimed at bone healing. *Bioact. Mater.* **2021**, *6*, 1479–1490, doi:10.1016/j.bioactmat.2020.11.001.
  141. Ghuglot, R.; Titus, W.; Agnihotri, A.S.; Krishnakumar, V.; Krishnamoorthy, G.; Marimuthu, N. Stable copper nanoparticles as potential antibacterial agent against aquaculture pathogens and human fibroblast cell viability. *Biocatal. Agric. Biotechnol.* **2021**, *32*, 101932, doi:10.1016/j.bcab.2021.101932.
  142. Wang, Y.; Lu, X.; Yuan, N.; Ding, J. A novel nickel-copper alternating-deposition coating with excellent tribological and antibacterial property. *J. Alloy. Compd.* **2020**, *849*, 156222, doi:10.1016/j.jallcom.2020.156222.
  143. Yang, C.; Zhang, C.; Liu, L. Excellent degradation performance of 3D hierarchical nanoporous structures of copper towards organic pollutants. *J. Mater. Chem. A* **2018**, *6*, 20992–21002, doi:10.1039/C8TA07973K.